AALBORG UNIVERSITET

AGGLOMERATION IN A POLYPROPYLENE COMPOSITE

Master's thesis

Patrick Kruse

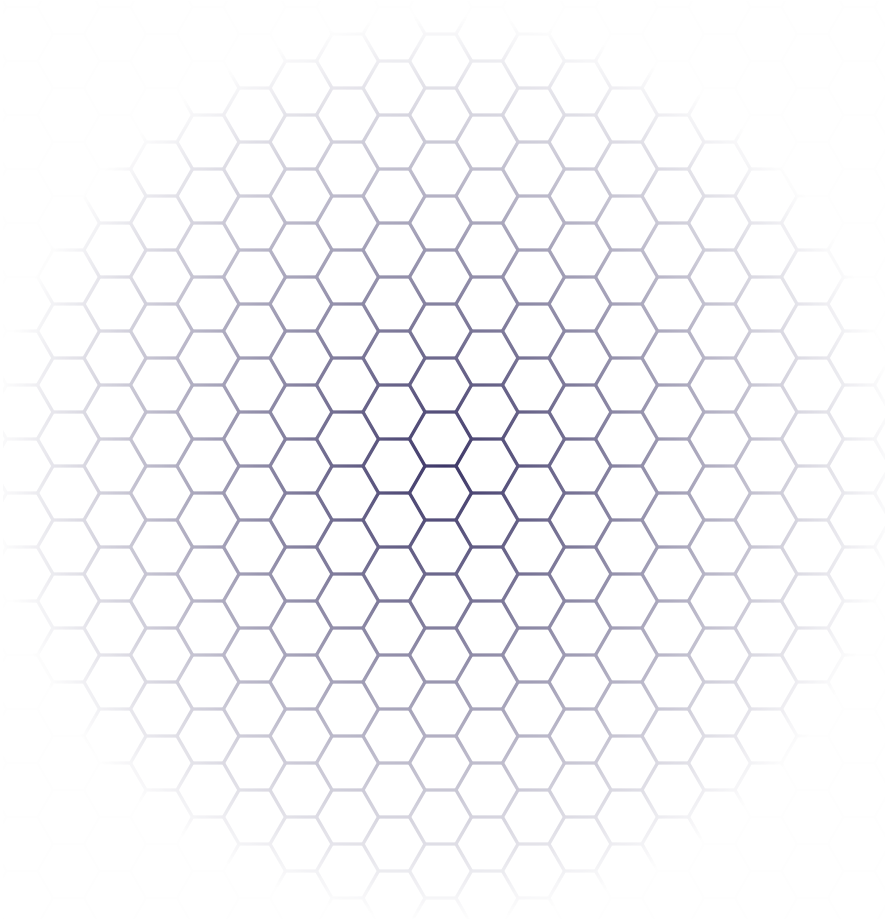

3rd of June 2020

Title: Agglomeration in a polypropylene composite
Semester: 10th
Theme: Master's dissertation
Project period: February 2020 - June 2020
ECTS: 30
Supervisor: Mikael Larsen

Department of materials and production
Fibigerstræde 16
DK - 9220 Aalborg Øst
Tlf. 99 40 85 32
snmp@mp.aau.dk
https://www.mp.aau.dk/

Synopsis

Electrochemically exfoliated graphene oxide has been used as a strength-enhancing filler in a polypropylene composite, but was found to exhibit abysmal levels of filler dispersion. This is thought to reduce the enhancing effects the filler can impart on the matrix, and this phenomenon is investigated and sought counteracted in this report, using a base-catalysed functionalisation procedure. A micromechanical model is also developed and it showed better dispersion coincided with higher stiffness increase, although only to a minor degree. The employed functionalisation procedure did not influence the agglomeration of the filler, but could increase the stiffness of the composite by around 60%. Composites of graphene oxide in polyvinyl-alcohol is also tested, as the filler disperses well in such a composite due to the particular method of mixing and/or the good chemical affinity between the two. A five-fold increase in stiffness was observed, compared to specimens of pristine polyvinyl-alcohol. From the aforementioned results it is concluded the poor degree of dispersion observed in polypropylene composites were not a result of the method of exfoliation, but rather the manner in which the filler was mixed with the polymer.

Synopse

Elektrokemisk exfolieret grafen-oxid har været anvendt som et styrkeøgende additiv i en polypropylenkomposit, men havde en høj grad af agglomerering. Dette reducerer den styrkeøgende effekt, additivet har på polymermatricen, og dette fænomen er undersøgt og forsøgt imødekommet i denne rapport, ved brug af en basekatalyseret funktionaliseringsprocedure. En mikromekanisk model er også udviklet, hvilket viste at bedre dispergering medfører større forøgelser af komposittens stivhed, dog kun i en mindre grad. Den anvendte funktionaliseringsprocedure kunne ikke ændre agglomereringen af additivet, men forøgede komposittens stivhed med omkring 60%. Kompositter af grafen-oxid i polyvinyl-alkohol testes også, fordi additivet dispergerer godt i en sådan komposit pga. den specifikke blandingsmetode anvendt og/eller de gode interaktionsegenskaber mellem de to. Sammenlignet med ren polyvinyl-alkohol havde kompositten fem gange højere stivhed. Fra de ovennævnte resultater konkluderes det at den dårlige dispergering set i polypropylenkompositterne ikke var et resultat af exfolieringsmetoden, men rettere måden hvorved fyldmaterialet inkorporeres i polymeren.

Patrick Kruse

AALBORG UNIVERSITET

Pages: 43
Appendices: 2

Contents

Chapter 1

Introduction

The work presented in this report is the continuation of experimental work already carried out, regarding the implementation of electrochemically exfoliated graphene in a polypropylene (PP) composite. This chapter will introduce the usage of nanofillers in a polymer composite, the exfoliation of graphene and present the important aspects of previous work. Claims made in the introduction is based on knowledge already acquired from literature studies in previous work[1].

1.1 Graphene as a strength-enhancing nanofiller

A variety of materials can be added to polymers in order to produce composites with enhanced or new properties whether it be mechanical, thermal, chemical or electronic. Carbon and glass fibres are typically implemented as a filler in polymer composites in order to improve their mechanical properties. These can be added in strictly oriented layers in order to strengthen the composite in certain directions, or they can be added in randomly distributed orientations, leading to an overall isotropic increase in strength. Strengthening fillers generally have high tensile strength and stiffness, that complements the flexible and ductile properties of the polymer. When a load is applied to the composite, part of the load is transferred to the stronger filler, thus contributing with carrying the load. Nanofillers are fillers with dimensions on the order of nanometers and are an attractive choice of strengthening material due to the incredibly high polymer/filler surface area of contact available. As such, higher degrees of load transfer is possible, meaning greater strengthening features. One of the typical problems arising from the use of nanofillers in polymers, is their tendency to not disperse throughout the composite, as they tend to prefer to clump together in agglomerates. The formation of agglomerates reduce the surface area available for load transfer, leading to little or no enhancing effects of mechanical properties, and can even produce diminishing effects. The degree of dispersion seem to be determined largely by the chemical affinity between polymer and filler - poor interphasial affinity mean filler particles prefer to migrate away from the polymer matrix and towards other filler particles. To combat these tendencies, functionalisation procedures are often utilised, where certain compounds are chemically attached to the filler in an effort to increase its affinity with the polymer or at least decrease its affinity for other filler particles. The usage of graphene as a nanofiller encounter similar problems regarding dispersion, but the material has become popular because of its many promising applications in polymer composites.

Graphene is a carbon allotrope and can be described as the constituent layers of commonly known graphite. A single sheet of graphene consist of carbon atoms arranged in a two-dimensional hexagonal lattice, each bonded through sp^2 hybridisation orbitals where the remaining p_z orbital protrudes normal to the lattice plane. This orbital is an ideal site for the formation of π-bonds between separate graphene sheets, which cause stacking of layers leading to the formation graphite. Individual graphene sheets have thicknesses on the order of nano meters and can have lateral dimensions on the order of micro meters, depending on how the material is obtained. It is possible to create graphene by chemical vapor deposition, a so-called bottom-up approach where the layer is built from constituent carbon atoms, or graphene sheets can be extracted in a top-down approach by the exfoliation of graphite. Exfoliation involves the pushing apart of graphene layers, in order to overcome the relatively weak interlayer π-bonds ($\sim 6\,\mathrm{kJ\,mol^{-1}}$)[2] and can be done in several ways. Chemical exfoliation involves the oxidation of graphite, typically done using a variation of Hummers' method[3], where a mixture of sulfuric acid and sodium nitrate oxidises the graphene layers which facilitate the reduction of anions (Hummers used potassium permanganate) that intercalate between, and push apart, layers. Electrochemical exfoliation works by the same principle of intercalation and layer separation, but uses an electrochemical cell to achieve the same. Graphite is used as anode in the setup, where dissociated electrolyte species intercalate between layers of graphene and subsequently reduce to gaseous bubbles that force layers apart. Other novel methods of exfoliation have

also been devised, but are only referred to in special cases and will not be considered in this text. Bottom-up approaches produce relatively large graphene sheets with few lattice defects, but is time-consuming and thus not scalable for industrial applications. Chemical exfoliation is quick, but also an aggressive procedure that typically damages graphene sheet structures. More importantly, the method require large amounts of toxic chemicals that produce various noxious gasses, while also leading to excessive heating during processing, further complicating the treatment. Electrochemical exfoliation still produces oxidised graphene (which will be referred to as GO), but is generally much simpler and does not involve the use of large amounts of toxic chemicals, while also being readily scalable for industrial use. Depending on the process parameters employed, electrochemical procedures can produce relatively high quality graphene sheets incredibly fast (on the order of minutes). Defining the quality of sheets naturally depend on their intended application, but is typically determined by their morphological characteristics. Lateral dimensions and their thickness (both found using atomic force microscopy) are of interest because obtained particulates tend to consist of several sheets still stacked on each other, which is unwanted. The number of sheets in a stack can be determined since the theoretical interlayer distance of $0.341\,\mathrm{nm}$ is well known. However, it is possible for the interlayer separation to increase following the attachment of functional groups during oxidation, and must be measured, typically done using x-ray diffraction. Preserving a high thickness to lateral size aspect ratio is critical for the effectiveness of graphene in a material composite, because such a shape can disrupt the "flow" of stress more efficiently. Graphene is an attractive nanofiller due to it having a high theoretical stiffness ($1\,\mathrm{TPa}$) and strength (σ_{ut} $=\sim 130\,\mathrm{GPa}$). Oxidation stemming from its extraction procedure can mar these mechanical properties by introducing defects in its lattice structure. Oxidised graphene can be reduced, removing residual functional groups, but does not guarantee the absence of defects in the lattice, so oxide groups are generally unwanted to begin with. Lattice defects allow for sheets to break into smaller fragments and generally reduce the mechanical properties of graphene and it is possible to assess the defect concentration using Raman spectroscopy.

1.2 Problems encountered in previous work

Graphene obtained from chemical exfoliation has previously been used as a nanofiller in a PP composite with the intention of improving its mechanical properties[4]. Electrochemically exfoliated graphene was later used similarly, in order to gauge the procedure in relation to chemical exfoliation[5]. Interestingly, the degree of particle dispersion was inferior as compared to composites containing chemically exfoliated graphene, and little to no change in mechanical properties was observed. The graphene was functionalised using octadecylamine in order to improve both dispersion and the mechanical properties. While the dispersion seemed to improve as a result of this treatment, the mechanical properties did not. Subsequent work[1] focused on the characterisation of graphene sheets obtained through electrochemical exfoliation of a variety of graphite sources. A graphite foil source was found to be optimal according to several criteria and was therefore implemented in a PP composite. Again the dispersion was abysmal, so a functionalisation procedure was employed, this time using stearic acid, which resulted in no significant change in dispersion and mechanical properties. From these investigations, graphene obtained from either exfoliation method was thought to behave differently either as a direct result of the exfoliation type or some other variance in the extraction method. Additional experimental work could help identify the differences in particles and understand how each extraction process influence these differences accordingly. There are several processing steps to investigate and a multitude of parameters to tweak and it is just a matter of selecting a particular area to begin investigating.

Chapter 2

Initial problem

GO is added to PP in order to produce a material with improved mechanical properties, as compared to those of pristine PP. There seems to be a large gap between the degree of improvements that *can* be obtained, as eluded to by several other works, and what is *actually* obtained in experiments. Understanding why such a gap exists along with the attempt at narrowing it, is the overarching problem sought dealt with in this report. Some of the primary factors influencing the improvements a filler material can impart on its surrounding matrix, is the filler agglomeration and interphasial bond strength, and are the areas of investigation to start at. From previous work it was found the agglomeration was deplorable due to the manner in which the GO was mixed with the PP. With this in mind, an initial preliminary experiment has been carried out where GO was mixed with polyvinyl alcohol (PVA), presented in Appendix A.1. Since PVA is water soluble, a suspension of GO in water can be thoroughly mixed with the polymer, and the resulting composite was found to have very low degrees of agglomeration. In previous work there was also a divide between the degree of agglomeration in composites containing GO obtained from either chemical or electrochemical exfoliation, the latter of which produced inferior composites. Through this initial experiment, it is clear that a good degree of dispersion (inverse of agglomeration degree) can be achieved even from electrochemically exfoliated GO. So in this report, focus will be directed towards reducing the degree of agglomeration of GO obtained by electrochemical exfoliation, in a PP composite, without comparing it to chemically exfoliated GO. As mentioned before, the intention is to ultimately produce a composite with markedly improved mechanical properties, as compared to the pristine PP material, and its performance in relevant tests will be used to gauge the success of the work.

Exfoliation	Rinsing	Sonication	Drying/scraping	Functionalisation
Time	Temperature	Time	Substrate type	Temperature
Voltage	Solvent type	Intensity	Force	Reaction time
Electrode separation	Solvent volume	Solvent type		Solvent type
Electrolyte properties		Temperature		
Convection		Cycling		
Graphite source				
Temperature				

Tab. 2.1 Processing steps and tweakable parameters in the method of GO production.

The properties of the GO itself is thought to be influencing its behaviour in a polymer, and depend largely on the manner in which it is produced. In previous work, the source of graphite was investigated in this regard, and it makes sense to now look at the method at which the graphite is converted to GO (in this case by electrochemical exfoliation). The specific method will be presented in a later section, but an overview of the processing steps is shown here in Table 2.1, along with some parameters that might be influencing the outcome of each step. This is the setup used in previous work and will be a starting point of investigation in this work. The steps shown encompass the entire process up until to the mixing of filler and polymer, which was found to be a difficult area to influence. This is also eluded to in the preliminary experiments, where PP was sought mixed with GO in a similar fashion as the PVA, and proved practically impossible. So while mixing is a critical step, it is left as is for now, and only the steps mentioned in the table above are considered. Of the many steps, the ones selected for investigation are the functionalisation and sonication due to several factors. Sonication is a complicated process and have been referred to as essential to the electrochemical exfoliation procedure, meaning it could be influencing the process heavily. Functionalisation is a popular avenue of research when working with the implementation of fillers in a polymer and proved ineffective

in previous work, so is sought improved upon in the present work. Investigation of the exfoliation step have been omitted from this work arbitrarily, but is naturally a hugely important step in the entire process. Rinsing is considered a superficial step and drying is practically unavoidable and impossible to influence directly, so these are also not considered in this work.

As mentioned before, the mechanical properties of the composite will be used as a gauge for the success of the investigation. While agglomeration by itself is thought to play a big role in the behaviour of the composite, other factors will inevitably be worth considering. In an effort to separate the effects of agglomeration from other effects, such as increased crystallinity, a micromechanical model will be constructed. The purpose of this model will be to study the effects that agglomeration in particular, has on the mechanical properties of the composite. Discrepancies between what is seen in the model and in experiments could then be considered to be a result of other effects than agglomeration. In summary, the key points of investigation in this report can be states as:

- Understand the mechanics of agglomeration of GO in a polymer
- Change the degree of agglomeration in a composite containing GO
- Find how agglomeration influences the mechanical properties of the composite

The investigation will begin with a literature study on topics selected based on experiences made in previous work and what is thought to be relevant in the current work.

Chapter 3

Literature study

Before defining exactly what work will be done in the present report, a comprehensive literature study into relevant topics will by carried out. The very first section will focus on the topics relating to the implementation of models and the rest will focus on topics relating to practical work, namely PVA, functionalisation and sonochemistry.

3.1 Graphene as a nanofiller

The nanoscale characteristics of the polymer-graphene material system and their influence on the macroscopic properties of the composite, are studied in this section. Material behaviour on this scale is considered on a molecular level, where individual atoms and their interactions with neighbours are taken into account through a variety of theoretical techniques. Three numerical modelling techniques are typically encountered in the literature, and can be briefly introduced as:

Molecular dynamics (MD)[6] The motion of atoms are described using conventional equations of motion where the interactions between atoms are described by potential functions. Such functions account for repulsion and attraction forces, that depend on interatomic separation.

Density functional theory (DFT)[7] The wave-like quantum mechanical behaviour of atoms can be described exactly by equations of wave mechanics. In this method, these equations are approximated by electron probability density functions, which are employed in a atomistic model to determine the structural properties of the system in question.

Molecular structural mechanics (MSM)[8] The axial stretching of interatomic bonds is represented by conventional spring elements also used in structural mechanics, where the stiffness in this case, is described according to some non-linear force potential function.

Characteristics of graphene

Since graphene is an arrangement of carbon atoms in a hexagonal lattice, it has a three-fold rotational symmetry and its mechanical properties depend on the load direction accordingly. Two principal directions can be identified; the armchair direction and the zig-zag direction, respectively highlighted in blue and red on Fig. 3.1, and both of these repeat at 60° intervals. Graphene may also be considered a two-dimensional material since it is one-atom thick, although it is debated what this thickness actually is[9]. Since the material is two-dimensional and exhibits orthotropic material properties due to its rotational symmetry, applied strains can be related to stresses using a simplified constitutive stiffness tensor:

$$\begin{Bmatrix} \sigma_1 \\ \sigma_2 \\ \tau_{12} \end{Bmatrix} = \begin{bmatrix} E_{11} & E_{12} & 0 \\ E_{21} & E_{22} & 0 \\ 0 & 0 & E_{66} \end{bmatrix} \begin{Bmatrix} \epsilon_1 \\ \epsilon_2 \\ \gamma_{12} \end{Bmatrix} \tag{3.1}$$

Its orthotropic material properties are typically analysed with respect to its principal directions because the layout of these produce the directional variations in properties. When loaded in the zig-zag direction, bonds are effectively sharing the load, while when loaded in the armchair direction, almost all of the load is carried only by bonds parallel to the load direction[10,11]. These variances in load distributions and the geometric configuration of the material constitutes its anisotropic properties.

Graphene is known to exhibit incredibly high stiffness and an E-modulus has been found theoretically to lie between 0.72-$1.3\,\mathrm{TPa}$[12,13], depending on the simulation procedure employed and the interatomic

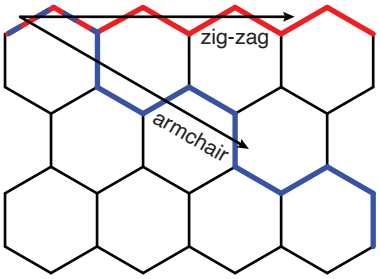

Fig. 3.1 Caption

properties applied in said simulation. Most estimations however, find a stiffness of around $1\,\mathrm{TPa}$ which also concurs with experimental data[14]. It has not been determined definitively which of the principal directions exhibits the highest stiffness, but most theorise them to be equal or with a difference of $\sim 100\,\mathrm{GPa}$. The stiffness in either direction has also been shown to converge to a similar value when sheets reach dimensions of $10\,\mathrm{nm} \times 10\,\mathrm{nm}$ and above[15,16]. In fact, several material properties were found to be dependent on the simulated sheet size, suggesting the discrepancies in material properties are due to localised effects and will even out when considered on a larger scale. Considering the relatively large size of most graphene sheets acquired in exfoliation methods (on the order of 0.1-$1\,\mu\mathrm{m}$[17–19]), the material at hand could be expected to exhibit similar stiffness in either direction. No particular interatomic mechanisms have been attributed to the variances in stiffness observed, but they are probably related to the restricted change of bond lengths and angles during deformation[20]. The shear modulus of graphene has also been determined theoretically to be around 285-$449\,\mathrm{GPa}$[15,16] and experimentally it was found to be $\sim 280\,\mathrm{GPa}$[21].

Several papers mention graphene to have a Poisson's ratio in the range 0.15-0.38 [15,16], which is a fairly wide span. There seem to be a divide between the values found. MSM models predict the value to be relatively high (0.22-0.38). DST models found a relatively low value (0.15-0.19). MD models agree somewhat with the MSM estimates, with values found to be 0.2-0.3. Determining why such discrepancies exist requires an extensive understanding of the models and without it, the selection of the "correct" parameter becomes a somewhat arbitrary task. DST models could be considered to account for more fundamental atomic interactions, while MSM and MD models provide an approximate, but more holistic estimate. In structural mechanics, the analyst is concerned not with atomic interactions, but the effects that can be observed on a macroscopic scale, leading the author to prefer the values determined by MSM and MD models. Other works found a so called auxeticity transition at excessive straining, above $6\,\%$, where the Poisson's ratio change sign to negative[22], and was seen to occur only when loaded in, and close to, the armchair direction[23,24]. This is an important effect to consider, should the composite simulation be found to undergo large deformations, albeit well into the region of plastic deformation.

So far only perfectly crystalline monolayer graphene has been considered, but in practice, graphene will inevitably contain defects in one form or another (ex. when in its oxidised form). As with other crystalline materials, graphene can exhibit defects to the lattice structure in the form of subsitutions, adatoms, vacancies and dislocations. Substitutional defects are never referred to in the context of chemical or electrochemical exfoliation of graphene and may be irrelevant for the given case. Doping (carbon substitution) of graphene with nitrogen and boron is an often encountered technique, used to improve the electrical properties of graphene, but require special treatments to implement[25]. As such, substitutional defects are assumed not be prevalent in the given case and disregarded of.

Vacancy defects are simply the absence of carbon atoms in the hexagonal lattice and can appear as a result of oxygenation and subsequent reduction[26]. Vacancies naturally weaken the graphene as they are sites of stress concentration, where premature crack initiation can occur. Decreases in stiffness and

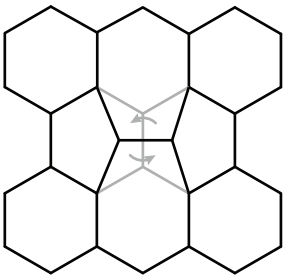

Fig. 3.2 Caption

ultimate tensile strength have been found to occur already at single atom vacancies, and the degree to which depended on the defect concentration[27]. Stiffness steadily decreased with increasing defect concentration, while tensile strength saw an initial decrease, but was somewhat constant above a defect concentration of $0.5\,\%$. Other works found that further variances in size, morphology and distribution of vacancies had only minor effects on the mechanical properties of graphene[10,28], indicating a high general resilience to the presence of vacancies. Depending on the location and orientation of the such defects, the growth of cracks can also be inhibited by defects, because defects lower the critical stress intensity factor locally[29]. Graphene was also found to have greater fracture toughness in the armchair direction[29]. This might be a result of topological defect formation during crack growth, that only occurs when the crack is propagating in the armchair direction, and has a hardening effect on the material[11]. Cracks are able to wander along either direction, but will be pure mode I if in the armchair direction and a mixed mode I and II if in the zig-zag direction[11].

Defects of the topological dislocation type, consist of disruptions in the hexagonal lattice structure, and take the form of bond rearrangements. Although countless dislocation types have been theorised, the most commonly encountered in graphene is the 5-7 dislocation or Stone-Wales defect[30]. This defect, shown in Fig. 3.2, typically appear at grain boundaries[31] and is the result of a $90°$ rotation of a single C-C bond. As with single-vacancy defects, a dislocation defect of this kind has been found to decrease both stiffness and fracture toughness of graphene sheets[27], possibly also due to stress concentration effects. When localised around a grain boundary however, these defects are able to strengthen the material, by disrupting the flow of stress across the sheet surface. The angle between adjacent sheets of graphene and the arrangement of defects influence whether or not the defects increase the effective material strength[31].

Adatom defects concern the covalent bonding of an external atom to the graphene, and depending on where the bond was formed, will alter the hybridisation state of the carbon it is attached to. These defects can be expected to be fairly prevalent on the graphene in the given case in the form of oxide moieties. When adatoms are bonded to the graphene surface, where carbons are already bonded with its three neighbours, a transition from sp^2 to sp^3 hybridisation would have to occur for the carbon atom. When adatoms are bonded at edges and vacancy defects, no change in hybridisation would occur for the carbon atom, because carbons at these sites already have less than three bonds. Sp^3 hybridised bonds are intrinsically weaker than the sp^2 kind, and would be expected to weaken the overall mechanical properties of the graphene. As such, the degree of passivation is an important characteristic, because graphene with higher degrees of passivation would be expected to contain larger concentrations of weaker sp^3 hybridised carbons. Hydrogenation of graphene was found to affect its strength only when the hybridisation state had been changed to sp^3[32]. In that case, a reduction in ductility of graphene was observed. This was because the formation of cracks occurred prematurely at weakened sp^3 bonds[10,32], and the formed cracks exhibited a smaller tip angle allowing the crack to grow more aggressively[32]. The additional spatial dimension of freedom has also been found to reduce the stiffness of graphene, because sp^3 bonds can rotate out of plane

as the sheet is deformed[33]. In the same paper, the site percolation threshold of a honeycomb structure was also considered, and at 30 % hydrogenation the stronger sp^2 bond network began to disrupt, suggesting a critical degree of passivation.

Graphene in a polymer material system

When included in a polymer material, the impressive mechanical properties of mono-layer graphene sheets are practically impossible to harness completely, due to the multitude of interaction effects involved. Strength enhancements of the composite are expected to appear because applied loads are transferred to the graphene, and the graphene is thus aiding with carrying some of the load. However, this requires for a large area of interphacial contact between graphene and polymer, along with strong interfacial bonding. Graphene tends to prefer to agglomerate, reducing the area available for contact, and the chemical affinity between graphene and polymer is typically very bad, meaning there is a weak interfacial bond.

Common polymers like polyethylene and polypropylene are crystalline in nature, meaning their macromolecules tend to conform into organised structures during solidification, because such configurations are energetically favourable[34]. The degree of crystallinity of a polymer influences its mechanical properties, as the crystal structures are more resilient to deformation, compared to an amorphous structure. Including graphene particles in the polymer allow for heterogeneous crystal nucleation to occur, which means crystal structures are more easily formed around said particles. As such, there is an area of high localised stiffness in the vicinity of the graphene particles. However, crystals are expected to be present scattered around the entirety of the polymer volume, so stiffening effects must be prevalent throughout the composite and in turn produce variations in the overall mechanical properties of the composite. So the effect is considered accounted for by simply increasing the overall stiffness of the overall polymer, that accounts for both amorphous and crystalline regions.

Upon inclusion in a nonpolar polymer composite, graphene is known to prefer to form agglomerates with neighbouring graphene particulates. This allows for sheets to be in direct contact with each other and, due to its good lubricity[35,36], will most likely be detrimental to the strengthening effects of graphene. When load is transferred from the polymer to the graphene, sheets may begin to slide instead of distributing the load across individual layers. Assuming the composite will inevitably contain graphene agglomerates, one is inclined to confer how graphene particulates interact when in direct contact with each other. This becomes a study of the tribological properties of graphene, where the effects of interlaminar forces are considered. As such, the mechanism of agglomerate formation will be disregarded of here and focus will be directed towards graphene-graphene friction.

In order to understand how graphene sheets in an agglomerate behaves, it is important to understand the concept of commensurability states in the context of crystal lattices. Commensurability regards the differences in the periodicity of atomic spacing when planes are stacked. When graphene sheets are perfectly stacked, an A-B stacking of layers can be observed, as shown to the left in Fig. 3.3, where the position of carbon alternates predictably with each layer. Such a configuration is said to be commensurable, because the periodicity of carbon atoms in the stacking direction can be described in simple terms. An equivalent, but incommensurable configuration can be seen to the right on Fig. 3.3, where the periodicity of carbon stacking is fairly complicated to explain.[37]

The carbon atoms in graphene are bonded by sp^2-hybridisation orbitals, meaning electrons in the p orbital is protruding normal to the sheet. These electrons are called π-electrons and are the cause of interlayer repulsion. When stacking graphene sheets, this repulsion is highest when the carbon atoms (and therefore also the electrons) are close to each other, meaning they prefer to configure in the well-known A-B stacking pattern. A-B stacking is the most energtically favorable configuration of graphene sheets, meaning some energy barrier has to be overcome in order disrupt this configuration, and attain interlayer sliding. When the energy barrier has been overcome, a less favorable state is obtained, and carbon atoms prefer to

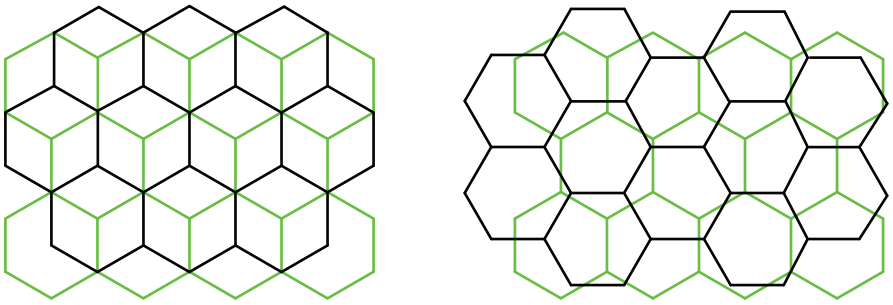

Fig. 3.3 Left: commensurable stacking of graphene sheets. Right: incommensurable stacking of graphene sheets.

slide into place again. As such, the interlayer friction takes the form of a stick-slip behaviour, where an initial force must be overcome, followed by a slipping of the carbon atoms into their preferable positions[35]. A friction constant can then be determined as the average force to be applied for one stick-slip period to occur. This force has been found to be much higher for commensurate graphene sheets, because the energy barrier is relatively high across the entire sheet considered[38]. In incommensurate sheets, there might be high local energy barriers, but they will be cancelled out by high local energy barriers of opposite sign, somewhere else in the structure. As such, sheets with incommensurate contact exhibit much lower friction constants as compared to commensurate sheets[38]. In an agglomerate, the configuration state of stacked sheets can be expected to be fairly complicated and vary locally, because sheets have been able to move and deform freely around each other. The main type of contact may be thought of commensurably stacked graphene sheets interacting incommensurably with another multi-layer graphene body. In such a case, the interbody friction will be higher with increasing layer count in either body and with decreasing interbody distance[39]. Edge step defects on either a body also increase the friction due to the local differences in binding energy across the step (also known as a Schwörbel-Ehrlich barrier)[40,41]. When the interbody contact occurs at grain boundaries sheets became corrugated (wrinkled), which in turn increase the interlayer friction[42]. Smaller grain sizes allow for more corrugation to occur, while hydrogenation of the exposed surface can suppress the corrugation[42]. Hydrogenated graphene have also been shown to exhibit higher friction forces than pristine graphene, and even higher for oxygenated graphene[43]. Interlayer and interbody sliding is generally considered detrimental to the strengthening effects sought, as the friction force is assumed to be considerably less than the rigidity of individual graphene sheets. If agglomeration is unavoidable, it would be attractive to reduce sliding by increasing the intraparticulate friction. This is achieved by hydrogenating or oxygenating the graphene and ensuring small grain sizes if the graphene is polycrystalline.

Graphene is a non-polar material, meaning there are no localised variances in the electronegativity accross the material surface, where intermolecular attraction might be induced. Of course the commensurable configuration of graphene layers allow for sheets to attract, but this is only true for very specific configurations. The interaction between similarly non-polar polymer macromolecules can therefore be assumed to be neither repulsive nor attractive. In order for load transfer to occur, the must be some force between the two phases, that counteract the shear stress that will be acting at the interface. Alternatively, mechanical interlocking effects could also allow for some load transfer, but such effects are not guaranteed to be present. Due to the large size and unpredictable ordering of polymer macromolecules, the contact state may be considered incommensurate and the friction relatively low. Functional groups can be added to graphene in order to induce interphasial interaction and the degree of interaction depend mainly on the polarity of the attached moiety and their concentration[44]. Non-polar moieties like $-CH_3$ and $-H$ and low-polarity moieties like $-NH_2$ and $-OH$ have weaker binding strength, while highly polar moieties, like $-O$, increased the binding strength[45]. Increasing the concentration of these moieties naturally enhanced their effects[45,46]. Localised graphitic (unfunctionalised) patches on other functionalised graphene sheets were

also found to have an strengthening effect, but only when the functional groups interacted strongly with the polymer[47]. Polycrystalline and wrinkled graphene was found to have improved interfacial strength, as compared to pristine graphene, due to the presence of higher number of adhesion points and greater opportunity for non-bonding interaction (mechanical interlocking)[48].

3.2 Polyvinyl alcohol

PVA is a soft thermoplastic commonly used in film[49,50], hydrogel[51,52] and fiber[53] composites and seldom in injection molding due to its poor thermal stability. Its monomer structure consist of vinyl alcohol(shown in blue on Fig. 3.4, and is impossible to prepare by direct polymerisation, because vinyl alcohol is unstable and will tautormerize into acetaldehyde. Poly vinyl acetate(PVAc) is instead used in a hydrolysis reaction as:[54,55]

$$(C_4H_6O_2)_n \xrightarrow[\Delta]{CH_4O} (C_2H_4O)_n + C_3H_6O_2 \tag{3.2}$$

Acetate groups on PVAc are converted to hydroxyl groups by methanol, which leaves behind methyl acetate as a biproduct. The degree of hydrolysis varies depending on how the reaction is performed, but the reaction product will always contain some unreacted acetate groups[56] that appear on the macromolecule as shown in Fig. 3.4. Hydroxyl groups influence the physical properties of the plastic because neighbouring macromolecules may form intra- and intermolecular hydrogen bonds[57]. PVA has a melting temperature of around 180-200 °C[58–60] depending on the degree of hydrolysis[61], which also influences its mechanical stiffness[57] and degree of solubility[62]. Polar plasticisers are used to reduce the stiffness of PVA, because they bond to the hydroxyl groups preventing the interaction between neighbouring macromolecules[57]. Residual acetyl groups are hydrophobic and disrupt the hydrogen bonding of macromolecules, resulting in a decrease in both mechanical strength and degree of crystallinity[55]. PVA is known for its solubility in water, and the hydroxyl groups contribute to this effect by rendering the polymer polar and hydrophilic. This property suggests polar fillers can be incorporated in the polymer to produce a composite with appreciable matrix/filler interaction. Graphene oxide is a suitable filler candidate because of its polar oxide groups, that are able to form hydrogen bonds with the hydroxyl groups on PVA ensuring good interfacial adhesion[52,61].

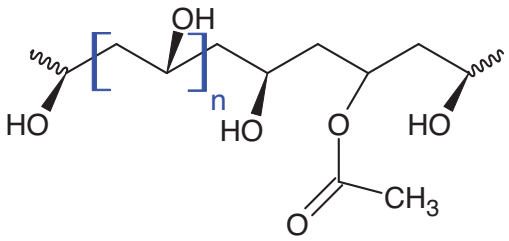

Fig. 3.4 Molecular structure of PVA with an unhydrolysed acetate group attached.

3.3 Functionalisation

Composite fillers are functionalised in order to modify their affinity with the matrix material. This can result in better interfacial bonding and a reduction in agglomeration degree, as functionalised particles may be less inclined to stick together. Stearic acid was used in the previous work as a functionalisation agent, and consist of an alkyl chain with a carboxylic acid head ($C_{17}H_{35}-COOH$) and is thought to react with epoxide groups present on GO[63,64]. The reaction is similar to the curing of certain thermoset plastics, where epoxide groups

are subject to an esterification by carboxyl groups[65–67], as shown on Scheme 3.3 - an ester is produced from an epoxide group subject to a ring-opening addition reaction with a carboxyl group. Following this reaction, it is possible for secondary reactions to occur, provided temperatures are high enough[66], where esters are esterfied by another carboxyl group as shown on Scheme 3.4. This reaction produces water as by-product, which can hydrolyse other epoxide groups[66] (Scheme 3.5), further increasing the concentration of carboxyl groups present on the GO. Since each reaction require for the ring-opening of epoxide groups, it seems the underlying mechanism involves the carboxyl-hydroxyl substitution, meaning epoxide groups are not necessarily required to functionalise GO, but hydroxyl groups already present on GO can be utilised. Since poor dispersion and thus no functionalisation was observed in previous work[1], the carboxyl-hydroxyl reaction must not have occured, indicating the importance of another factor.

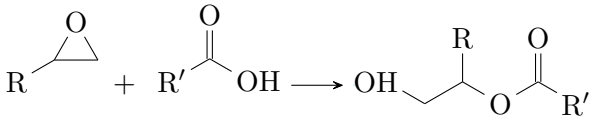
(3.3)

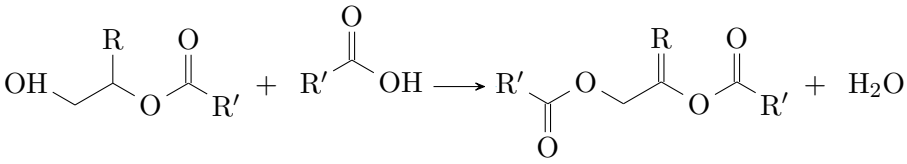
(3.4)

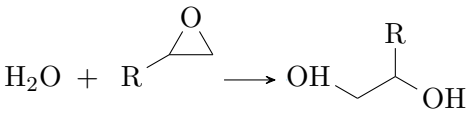
(3.5)

Stearic acid is considered a weak acid (pK_a of around 8-9.5[68]), so it dissociates into its carboxylate conjugate only to a lesser degree, and the presence of this conjugate is important for the carboxyl-hydroxyl reaction to occur. Carboxylate is a nucleophile and desires to accept the hydrogen in the hydroxyl group, but due to the high pK_a value of stearic acid, this conversion is not heavily favoured and the carboxyl-hydroxyl reaction rate is low[66,67]. Catalysts have been used in the literature to complement functionalisation procedures using Stearic acid[64,69] and serve different purposes depending on the substance used. Basic catalysts react with stearic acid, as shown on Scheme 3.6, where carboxylic acid is deprotonated to a nucleophilic carboxylate. Acidic catalysts react with GO, as shown on Scheme 3.7, where an epoxide group is converted to a hydroxyl group. Bases are preferred catalysts in curing thermoset reactions, as it suppresses the homopolymerisation of epoxy[66], where epoxide groups are connected with each other (Scheme 3.8) - an epoxide group reacts with an esterified epoxide to produce an ether, containing only a single carboxyl group. Ethers can be considered unwanted in the given case, as multiple epoxide groups are spent for the attachment of a single stearic acid molecule, effectively reducing the degree of stearic acid functionalisation.

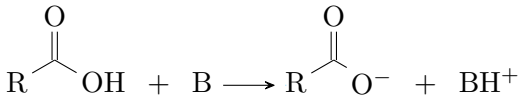
(3.6)

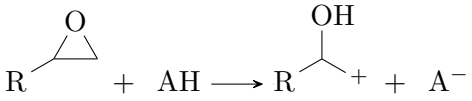
(3.7)

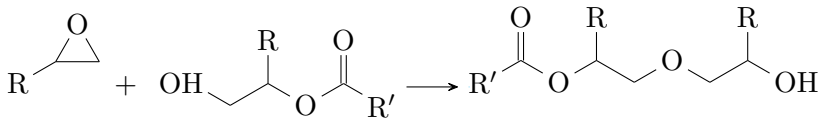

(3.8)

In the functionalisation procedures employed, stearic acid was dissolved only in ethanol which does not facilitate deprotonation, rendering the molecule unable to react with hydroxyl groups on GO. Stearic acid can be pretreated using an equimolar concentration of base, such as NaOH, to produce a salt capable of reacting with hydroxyl groups and possibly also open epoxide groups without the aid of acids. Acids are undesired due to the homopolymerisation effect mentioned before, although their inclusion in the procedure could be an interesting avenue of investigation, since acidic catalysts have been used in the literature before.

3.4 Sonochemistry

This section is based on Bhangu[70] and Ashokkumar[71].

Sonochemistry involves the chemical reactions initiated by ultrasonic agitation of a liquid. Ultrasonic waves themselves are unable to interact with molecules and intramolecular bonds directly, due to their relatively high wavelength, as compared to the size of said molecules and bonds. The waves instead influence chemical processes through acoustic cavitation, where bubbles are formed, grow in size and collapse resulting in large local differences in temperature and pressure. These differences can in turn affect the molecules in the agitated solvents. Liquids can be agitated by use of sonication equipment, which impart acoustic vibrations to the liquid using piezoelectric elements. Acoustic waves produce cyclic variations in pressure

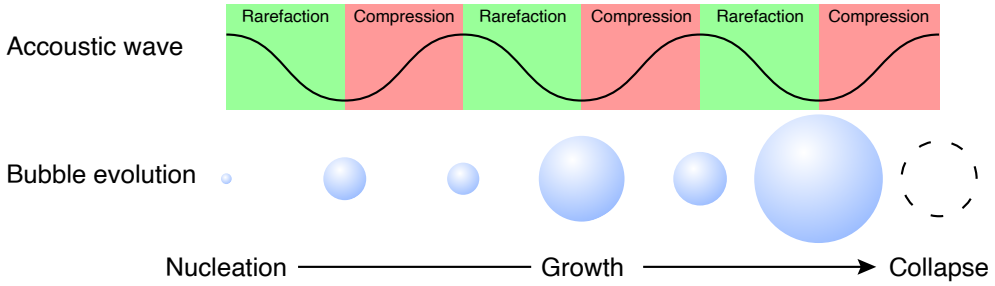

Fig. 3.5 A bubble subject to an acoustic field grows by rectified diffusion.

in a liquid, which result in the formation of bubbles, provided the amplitude is high enough to overcome the intermolecular bonds of the liquid. However, heterogeneties such as free gas bubbles and gas molecules trapped in solid impurities can drastically reduce the pressure amplitude required for bubble formation. Once a nucleus has been formed, bubbles can grow as a result of coalescence or rectified diffusion. Coalescence is the simple joining of two or more bubbles to form a larger bubble. Rectified diffusion involves the flow of mass from the bulk liquid into the bubble, due to the fluctuating pressure field that is affecting the bubble, and is illustrated on Figure 3.5. Two main effects are involved in this process - the area effect and the shell effect. A bubble in a liquid expands when its surrounding liquid experiences a negative pressure during the rarefaction (expansion) half-cycle of the acoustic field. This results in a low internal bubble pressure, which sucks in evaporated liquid and dissolved gas molecules from the surrounding liquid. During the compression half-cycle, the bubble reduces in size and the internal pressure increases, pushing out gas/vapour molecules back into the surrounding liquid. Since less surface area is available for mass transport during the compression half-cycle, there is a net gain of molecules in the bubble. This is known as the area effect. The shell effect considers the changes in gas concentration in the diffusion layer (shell)

of the bubble. During the compression half-cycle the shell thickness increases, leading to a decrease in gas concentration in the shell. The concentration of gas is now higher inside the bubble, compared to the shell, meaning gas will flow out, and since the rate of diffusion is proportional to the gradient at the interface, the flow rate is relatively low. In its expanded state, the shell is thin and its gas concentration is high compared to inside the bubble, meaning gas flows into the bubble, and with a steep concentration gradient, the flow rate is relatively high. This results in a net flow of gas into bubble, because the diffusion gradient is steeper when gas flows into the bubble, compared to when it flows out.

The bubble grows until a critical size (on the order of micro meters) has been reached, where the natural bubble oscillation frequency matches that of the driving acoustic waves. During the next vibration cycle the wave amplitude, and therefore also bubble radius, can increase drastically due to resonance effects and the bubble becomes unstable and implodes. This implosion is a sudden (μs - ns) almost adiabatic process where pressures rise to over $100\,\mathrm{MPa}$ and temperatures to over $5000\,\mathrm{K}$ inside the bubble. Drastic increases in pressure lead to the formation of shock waves, which travel through and imparts large shear stresses to the surrounding liquid. Since the considered bubble volume is fairly small, the produced heat quickly disperses in the liquid and only the bubble-liquid interface region experiences high temperatures. Gasses and vapours inside the bubble dissociate during the collapse, as a result of the high temperatures produced, and leads to the formation of molecular oxidants. In an air-saturated solution of water, the generation of nitrogen dioxide can occur, which through further reaction with water can form nitric acid resulting in a decrease in solution pH. Following the bubble collapse, its radius oscillates in a decaying radial bouncing motion which stabilises and the bubble can then grow in size once again, repeating the entire cycle.

Chapter 4

Problem statement

Many topics were considered in the literature study, relevant to both theoretical and practical work, and it can be clarified which areas of investigation will be followed. The theoretical work examined seem to focus mostly on microscopic interactions between individual atoms on a molecular level, and it is suggested that certain effects might disappear when moving to larger scales. The microscopic phenomena are also difficult to reproduce in any practical sense, which makes it impossible to verify the validity of the methods used to develop the model. Instead of developing a model on a molecular level like was seen in the literature study, a numerical continuum mechanical model is opted for instead. In such a model, the composite in question is imitated by developing a so-called representative volume element, where factors such as agglomeration and interfacial bonding can be taken into account, without considering atomic interactions. The elastic properties of said element can be evaluated and those are assumed to be representing the elastic properties of the composite on a macroscopic level. To verify the model, predicted properties can then be compared to results gathered from practical experiments such as tensile tests. To further specify the developed model, only agglomeration effects will be considered in the present work.

Critical information about the functionalisation procedure was also procured in the literature study and it seems obvious, that an attempt should be made at improving the procedure employed so far. A catalyst was found to be crucial for the effectiveness of the procedure, and that basic compounds (as opposed to acidic) were preferred catalysts. Additionally, an acidic catalyst have practically already been utilised in the form of sulfuric acid present in the electrolyte during exfoliation of the graphite, as will be presented shortly. So attempting a functionalisation procedure using an acidic catalyst is deemed unnecessary and experiments will therefore only make use of a basic catalyst. The functionalised material will be characterised by the use of infrared spectroscopy, where it is possible to determine if the desired functional groups have been attached to the material.

The sonochemical part of the literature study provided an explanation of the microscopic phenomena occurring during the sonication of GO. These effects will not be easily observable in a practical sense, and it is generally thought sonication will be difficult to relate to the characteristics of the GO produced. Only some superficial experiments can be thought of, which will be carried out, but attention will otherwise be directed elsewhere. From the preliminary experiments the usage of GO in PVA proved an attractive area of investigation, as the composite basically contrasts the behaviour of GO in PP. From the literature study it is now known the polarity of the polymer is most likely the cause of this, and the inclusion of GO might increase the mechanical properties of the composite significantly. This composite of PVA is effectively the optimal case that is sought after in the PP composite, and experiments with the PVA composite will be carried out in order to confer how the GO would ideally be interacting with the PP composite. Additionally, a small experiment studying the agglomeration process in a polymer composite will be carried out using PVA.

Overall the work will be covered in two parts - practical experiments and the development of a theoretical continuum mechanical model. Experiments will focus primarily on the functionalisation of GO and its effects on agglomeration in a PP composite. A PVA composite containing pristine GO will also be analysed and compared to the performance of the PP composite. The theoretical model will be constructed so as to imitate the produced composites in regards to agglomeration only. Tensile tests on composites will be used in junction with the results from the model, to gauge the influence of varying degrees of agglomeration. Additionally, some minor experiments revolving other agglomeration phenomena will be carried out; the effects of sonication on agglomeration in a suspension, and the formation of agglomerates in a PVA solution.

Chapter 5

Methods

Several experiments have been thought up for each of the areas of interest presented in the problem statement. A more in-depth explanation of what is sought investigated in the experiment is presented in this chapter, along with a thorough description of the processing steps employed in the design of the experiments. In the last section, scripts and methodologies relevant to the theoretical model developed, are presented.

5.1 Practical work

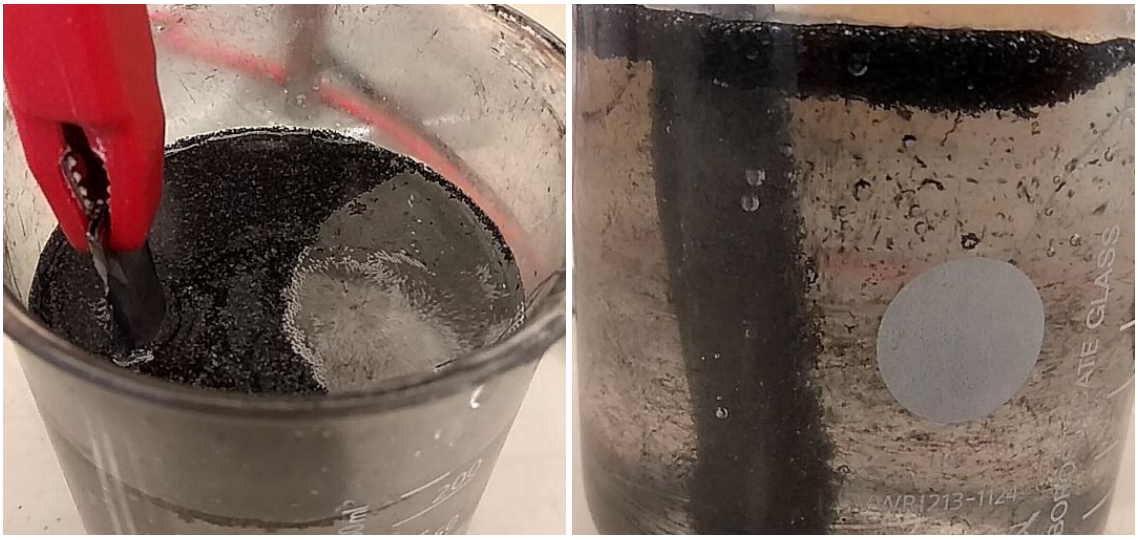

(a) **(b)**

Fig. 5.1 The electrochemical exfoliation procedure.

Graphene oxide production

GO used for all experiments was obtained by electrochemical exfoliation, and the setup was as described in previous work[1], but is outlined here again. A rolled up sheet of $\sim 10\,\mathrm{cm} \times 7.5\,\mathrm{cm}$ ($\sim 1.5\,\mathrm{g}$ graphite foil was used as anode and a platinum-alloy wire as cathode. Both were submerged in an electrolyte consisting of a $225\,\mathrm{mL}$ solution of $0.1\,\mathrm{mol}$ H_2SO_4 (sulfuric acid) and a current was passed through the system. Initially, a voltage of $2\,\mathrm{V}$ was held for $10\,\mathrm{min}$ whereafter a voltage of $10\,\mathrm{V}$ was kept until all of the graphite was consumed, this took about $2\,\mathrm{h}$. A picture was taken while exfoliation was occurring, about $30\,\mathrm{min}$ into the procedure, seen on Figure 5.1. On Figure 5.1a, the folded up graphite foil can be seen clamped to the left while the platinum-alloy wire can be seen surrounded by bubbles. On Figure 5.1b, the graphite can be seen submerged and attacked by the electrolyte. Small fragments of graphite/GO can vaguely be seen leaving its surface, while many fragments can be seen floating around in the electrolyte. It is unknown whether or not these are graphene agglomerates, but they disperse completely following a sonication procedure, evidencing the importance of the sonication step. An expansion of the foil was never observed, even though this was to be expected according to the literature. The fragments tended to move away from the wire cathode, suggesting they have a negative charge, which is repelled by the negative charge of the cathode, or that they are simply being pushed away by convection due to heavy bubble formation. After exfoliation, the GO was filtered off and rinsed several times with deionised water, dispersed in either ethanol or water,

depending on what it is to be used for, and sonicated using a $460\,\mathrm{W}$ rod sonicator for $30\,\mathrm{min}$ at $70\,\%$ power. The suspension acquired after sonication was a black and completely opaque liquid, with a viscosity similar to the solvent used, although at high GO concentrations, the suspension was rather viscous. The GO yield immediately after exfoliation was around 67% and a minute amount would be lost during subsequent rinsing steps, from being caught in the filter. The final yield is probably around 65% although it was never definitively determined, as the GO was kept in a liquid suspension at all times, complicating an assessment of its mass.

Functionalisation

GO produced via the above mentioned exfoliation method was subjected to a functionalisation procedure involving stearic acid and NaOH. A solution of $100\,\mathrm{mg}$ stearic acid dissolved in $20\,\mathrm{mL}$ ethanol was prepared along with a solution of $14\,\mathrm{mg}$ NaOH in $20\,\mathrm{mL}$ deionised water. The concentration of the two solutions are equimolar ($\sim$2.8 mol), which was important for ensuring all the stearic acid would be dissociated. Both solutions were mixed together and a suspension of $150\,\mathrm{mg}$ GO in $20\,\mathrm{mL}$ ethanol was added. The mixture was left with stirring overnight. Next day the mixture was filtered off using vacuum filtration and the solute was suspended in around $100\,\mathrm{mL}$ ethanol, heated in order to dissolve leftover stearic acid, and filtered again. This dissolution, heating and filtering was repeated twice in order to ensure most of the unreacted stearic acid was removed completely. The final solute was again suspended in ethanol, ready for use in experiments. Graphene oxide functionalised using this method will be referred to as "NaOH-GO".

Composite preparation

In previous work, polymer and *powdered* GO was melt mixed in a twin screw Xplore MC 15 micro compounder. In this work, polymer beads are submerged in a suspension of GO in ethanol, which is left to dry overnight, leaving beads coated with GO, as shown on Figure 5.2. From the image it is also evident, that a substantial amount of GO has covered the surface of the container, and it was found that only about half of the GO was covering the beads. As a result, the actual weight percentage of graphene in the composite is half of what is actually wanted. Nevertheless, a mixture of $15\,\mathrm{g}$ PP (Moplen HP400R by Lyondyell Basell, datasheet provided in Appendix A.2) and $\sim$750 mg GO was added to the compounder. The melt was mixed for $10\,\mathrm{min}$ at $200\,^{\circ}\mathrm{C}$ with a screw speed of $100\,\mathrm{rpm}$. Moulding of tensile specimens was carried out as in previous work using a Thermo Scientific HAAKE Minijet II. The melt is held at $220\,^{\circ}\mathrm{C}$, injected into a $70\,^{\circ}\mathrm{C}$ preheated mould using an injection pressure of $300\,\mathrm{bar}$ held for $10\,\mathrm{s}$, followed by a post-pressure of $100\,\mathrm{bar}$ held for $10\,\mathrm{s}$. Specimens have dimensions in accordance with ISO-527 type 5A. The same procedure was employed for preparing composites of PP and the functionalised NaOH-GO.

Fig. 5.2 Polymer beads coated with graphene (bads were originally semi-translucent white).

Preparation of PVA composites

In order to study the effects GO has on a compatible polymer such as PVA (due to its similar polarity and preferable method of mixing), tensile specimens of PVA were prepared. The PVA used had a degree of hydrolysis of 86.5-89 %. PVA is a very different material to work with, compared to PP, as it can not easily be injection moulded into a specimen of reproducible dimensions. Instead PVA can be dissolved in water, poured into a mould of the desired dimensions and left to dry. There are a multitude of problems with this, as the PVA tend to wrinkle and shrink during the evaporation of the water, and the solution contains air bubbles that are practically impossible to remove completely. This means specimens will inevitably have large variations in appearance, but samples were prepared regardless of this fact.

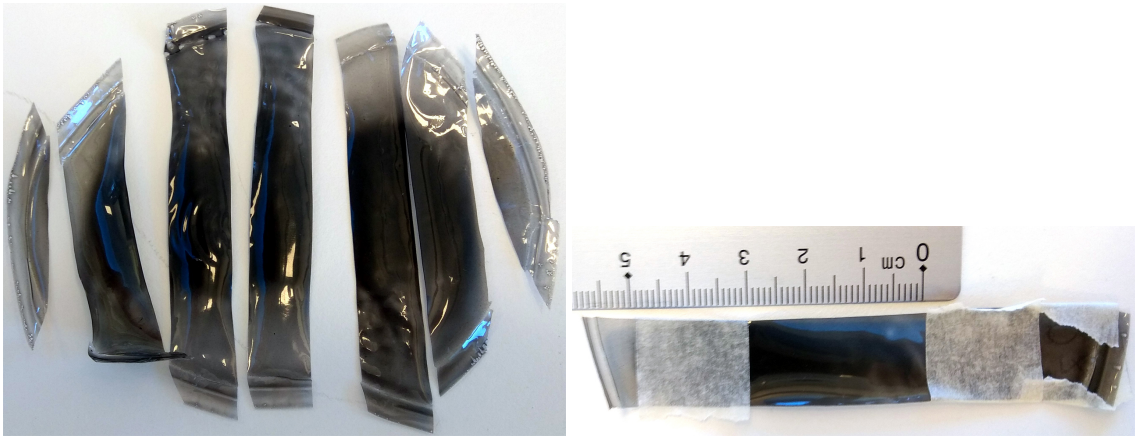

(a) **(b)**

Fig. 5.3 Prepared films of PVA/graphene composites.

A solution of 5 g PVA in 100 mL deionised water was prepared and poured into two plastic petri dishes (∼10 cm in diameter) and left to dry overnight. This was also done using a solution where around 50 mg GO had been added. When the solution was completely dry, a thin film of PVA was left on the surface of the petri dishes, which could be peeled off and cut to size. Films were cut into rectangular sticks using a box cutter, being careful not to introduce any cuts that could act as local sites of stress concentration. Specimens were cut to a width of 15 mm. The cut sticks containing GO can be seen on Figure 5.3a and it is evident the filler have not been evenly distributed throughout the films, thought to be a result of convection of water during evaporation. A majority of the filler is concentrated around the centre of the sticks, and this fact is taken advantage of by only subjecting this section of material to strain during tensile testing. As such, a gauge length of 30 mm was placed in the centre of each stick, marked with masking tape as shown on Figure 5.3b. This ensures all sticks have a similar amount of filler contained in the region subject to strain, making them more comparable. The thickness of the sticks was measured in the centre of their gauge length and will be presented in the relevant part of the section covering the results of tensile tests.

Agglomeration in PVA

Agglomerates are thought to form during the solidification of the wet mixed PVA/GO solutions, and a small experiment will be conducted in order to investigate this. PVA macromolecules could be preventing GO particles to agglomerate by locking the particles in place mechanically, since polymer material is surrounding the particles during solvent evaporation. This is investigated by depositing the PVA/GO solution from the above composite preparation onto a watch-glass and inspecting the fluid in an optical microscope (Zeiss Axio Imager M2m, which is used for all optical microscopy work). The solution is left to dry

overnight while images are acquired automatically every minute. In this manner it is possible to observe how the particles are moving around and forming agglomerates. The timelapse was carried out over a $24\,\mathrm{h}$ time span.

Sonication

Sonication is a crucial step in the exfoliation procedure, but is also used every time GO has to be evenly dispersed in a suspension, which is necessary if exfoliated GO is kept in storage long enough for particles to come out suspension (several weeks). A sonication treatment reduce the agglomerated solids to finely dispersed particles due to sonochemical phenomena (described in Section 3.4). The degree of dispersion in the liquid is somewhat irrelevant if the liquid is to be used in a PP composite, as the particles are allowed to settle on polymer beads, and thus they inevitably agglomerate. However, when used in a PVA composite, that is prepared by wet mixing, the degree of dispersion in the sonicated liquid (for the case of PVA composites, water) is an important factor. The size of agglomerates observed in the PVA composite is practically governed by the effect of the sonication, so it is interesting to consider the efficacy of the sonication procedure. When sonication is carried out, wattage and time are the primary variables that can be controlled and the influence of these are the focus of this experiment. The solution have been observed to become heated during sonication and temperature might also be an important, less controllable factor. Temperature is probably difficult to control, as the sonication is quite vigorous even at low power and no cooling equipment is thought to be able to counteract the heating. Instead the temperature is assumed not to affect the degree of dispersion, but will be monitored throughout the experiments. Four sample solutions of water and GO, each containing the same amount of GO, will be sonicated using four combinations of time and power. Time will be either 10 or $50\,\mathrm{min}$ and power will be either 20 or 60%. Immediately after sonication, suspensions are deposited on a watch-glass and inspected in a microscope.

Tensile testing

Since the material properties of composites of PP and PVA were different, their tensile tests were also carried out differently. PP samples were tested according to ISO-527 which among other things required for the E-modulus to be determined at 0.05-$0.25\,\%$ strain, where the strain rate should be 1% of the gauge length per minute, or $0.2\,\mathrm{mm\,min^{-1}}$ in this case. Outside this window, the strain rate was arbitrarily chosen to be $10\,\mathrm{mm\,min^{-1}}$. For the PVA composites, it was chosen to have a constant strain rate of $10\,\mathrm{mm\,min^{-1}}$ throughout the experiment, due to the high elasticity of the material. At low strain rates, there would be no appreciable force measured, because the material would so easily give way, eluding to it having a low stiffness. Furthermore, the modulus of elasticity would have to be determined using an extensometer, that could measure strains accurately. Due to the high elasticity of the material, the extensometer simply did not read any strain during loading, and it was necessary to resort to using the position of the crosshead, which is naturally not as accurate. Both composites were tested using a Zwick Z100.

5.2 Theoretical work

The main focus of the model will be to create a representative volume element (RVE) that imitate the agglomeration observed in the tested specimens. Using the "material designer" tool in Ansys Workbench software, it is possible to construct a custom volume element and compute its effective mechanical properties. This volume has to be built from a CAD-model which becomes a tedious task because each agglomerate must be placed and drawed manually. Agglomerates are somewhat random in appearance and are also distributed in the composite randomly, which can be taken advantage of in a script capable of generating the material system in a pseudo-random manner. The idea is to create instructions of drawing

shapes, which the Ansys software can interpret, so the RVE is drawn automatically. It is desired for the instrucctions to be based on parameterised properties, so the RVE can be varied according to how the actual material system appears, for example by being able to vary the volume fraction. The material system in question is fairly complicated and several shortcuts have been taken in order to be able to construct a RVE. Most importantly, the entire material system is modelled only in two dimensions which inherently means agglomerates can only be considered to be flat. The out of plane stiffness of the simulated composite will therefore be disregarded of completely, only transverse and perpendicular stiffnesses are considered. When only a slice of the composite is considered, possible orientations of agglomerates will also be lost, meaning the size distribution of agglomerates will most likely be wrong. The orientation of agglomerates are also not accounted for and agglomerates are therefore considered completely isotropic. In the actual composite, a volume fraction might be determined, which in terms of this model can be represented only as an "area fraction". With these points considered, a script capable of outputting instructions of drawing shapes is presented. The code presented in the proceeding sections are commented on as it was deemed fit, but all lines of code presented in a section belong to the same script. All but the final script have been written in MatLab software.

Characterising composite specimens

This procedure simply scans an input image and return areas and positions of detected clusters of agglomerates. It is intended for an input image to be of a composite containing particles that are easily distinguished from the surrounding material. What is meant by this will become evident in the following chapter, where microscopy images of composites are presented. First the image is loaded and converted to a binary image, meaning pixels are identified to be either black, if it belongs to a particle, or white if it does not, according to a threshold value. Should the brightness of a given pixel be higher than the threshold value, the pixel is seen as completely white, otherwise it is completely black. This is important for the cluster detection procedure, as it can only distinguish between black and white pixels. The threshold value must also be picked carefully in order to extract only black agglomerates, and not grey artefacts from scratches and the like.

```
function [areas,xs,ys] = GetImageClusters(doplotting) % Declaration of this function

files = dir('*.jpg'); % Get structure of all .jpg files in directory
findex = 1; % File index to load
fn = files(findex).name; % Store its name
im = rgb2gray(imread(fn)); % Store the image as a matrix

imbw = imbinarize(im,0.2); % Convert image matrix to a binary representation
imbw = imcomplement(imbw); % Invert the image matrix
```

Next, a region of the image is extracted for inspection. This is done to omit the specimen edges or cracks that may have appeared during sanding/polishing of the specimen, which are clearly not agglomerates and should therefore not be detected by the procedure.

```
pm = length(imbw(1,:))/12; % Pixel/length ratio
inssize = 10; % Size of inspection window in mm (window is square)
% The window is offset so it is placed in the center of the image
insoffx = round((length(im(1,:))-(pm*inssize))/2);% Pixel offset x of inspection window
insoffy = round((length(im(:,1))-(pm*inssize))/2);% Pixel offset y of inspection window
mxlim = [insoffx round(insoffx+inssize*pm)]; % Convert offset to matrix entry
mylim = [insoffy round(insoffy+inssize*pm)];
iminsp = imbw(mylim(1):mylim(2),mxlim(1):mxlim(2));% Area to inspect

CC = bwconncomp(iminsp);% Get clusters
dim = size(iminsp); % Dimensions of inspections windows
```

If the program is told to plot the scanned image, specified by the `doplotting` variable in the very first line of the script, the following lines will be executed. The input image is simply shown to the user, along

with the section of the image that has been analysed and the detected clusters. Such an image will also be presented in the following chapter.

```
%% Plotting
if(doplotting)
   figure
   imshow(im) % Show the input image
   hold on

   % Create overlay image
   overlay = zeros(dim(1),dim(2),3); % Initialise the overlay
   overlay(:,:,1) = 1; % Set its color (red)
   imalpha = iminsp; % Overlay image is equal to the inspection area
   h = imshow(overlay,'XData',mxlim,'YData',mylim); % Overlay it on current figure
   set(h, 'AlphaData', imalpha*0.6);% Set its transparancy

   % Plot square based on matrix to inspect
   hold on
   plot([mxlim(1) mxlim(2) mxlim(2) mxlim(1) mxlim(1)],[mylim(1) mylim(1) mylim(2) mylim(2)
        mylim(1)],'color','red','lineWidth', 2)

   % Save plot
   saveas(gcf,'outputimage','png');
end
```

Finally, some calculations are done on the clusters identified, in order to get the correct units and dimensions. Each agglomerate is stored as a matrix of pixels, designated by the number each pixel is known by, and this is an intrinsic property of the `bwconncomp` function. This number is counted from the upper left corner of the image going down and to the right, i.e. the very first pixel has number one, while the pixel to the right of it has number one plus the height of the image. This fact is utilised to convert the pixel number to an x or y coordinate, where x goes from left to right, and y goes from up to down.

```
%% Calculations
areas = cellfun(@numel,CC.PixelIdxList)/pm^2; % Get the area of each cluster (with the unit specified in pm)

% Get the x and y coordinate of each cluster
xs = zeros(1,length(CC.PixelIdxList)); % Initialise matrices
ys = zeros(1,length(CC.PixelIdxList));

for i=1:length(CC.PixelIdxList) % For all detected agglomerates
   mat = cell2mat(CC.PixelIdxList(i)); % Gets the matrix of pixel numbers for the agglomerate

   xs(i) = floor(mat(1)/dim(2))+1; % Convert number to a x coordinate
   ys(i) = mod(mat(1),dim(2)); % Convet number to a y coordinate
end
```

The acquired data is now ready to be used in the main program, but before it is presented, the agglomerate representation procedure is presented first.

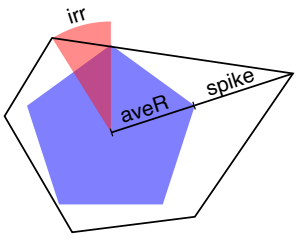

Fig. 5.4 How parameters are influencing the vertices of a polygon with `vertn` = 5.

Representing an agglomerate

While agglomerates can take on fairly complicated geometries, they are simplified by considering them as regular polygons, with some alterations. A polygon of `vertn` vertices is generated according to an average

radius, `aveR`, and two parameters; irregularity, `irr`, and spikiness, `spike`. The irregularity parameter controls how much a vertex is allowed to wander along the periphery of the enclosing circle. Spikiness controls how much a vertex is allowed to wander away from the average radius of the enclosing circle. The two parameters have been illustrated on Figure 5.4. Polygons are stored in a matrix of vertex coordinates in a manner that groups vertices together in line segments, which is required for Ansys to correctly parse the information.

```
function final = GeneratePolygon(vertn, aveR,irr,spike) % Declaration of this function

px1 = zeros(1,vertn); % Initialise matrix containing x coordinates
py1 = zeros(1,vertn); % Initialise matrix containing y coordinates

for i=1:vertn % Create vertn number of vertices
   ang = deg2rad(360/vertn*i) + rand*irr; % Angle to place vertex at
   r = aveR + rand*spike; % Radius to place vertex at
   px1(i) = r*cos(ang); % Convert angle and radius to cartesian coordinates
   py1(i) = r*sin(ang);
end

% Shift the polygon so it has no negative numbers
px1 = px1 - min(px1);
py1 = py1 - min(py1);

% Create a second matrix of the same points, shifted one column to the right
% This is done to allow for representation of the polygon as line segments
px2 = circshift(px1,-1);
py2 = circshift(py1,-1);

final = [px1 ; py1 ; px2 ; py2]; % Return the complete matrix of all line segments
```

It is now possible to generate an agglomerate and they must now be created and distributed across a canvas, representing a composite section.

Drawing a system of polygons

The following code governs the size and spatial distribution of agglomerates in a single plane of the composite. In that regard it is necessary to find a suiting probability density function for the x and y coordinates of each agglomerate along with a function for their sizes. This is were the data collection script presented in the beginning of this chapter comes into play, as said data can be fitted to a given probability function. In order to fit the functions, a suitable probability distribution must be identified, which is done by inspecting the histogram of coordinates and areas, shown respectively in Figure 5.5a and b. The coordinates seem somewhat uniformly distributed and can be estimated by a uniform distribution function, while the areas have a strong preference for smaller areas and another type of distribution function must be selected. A beta distribution function is fairly versatile and should be able to represent the observed histogram well. In its standard form it is given as

$$P(x|\alpha,\beta) = \frac{x^{\alpha-1}\cdot(1-x)^{\beta-1}}{B(\alpha,\beta)}, \qquad B(\alpha,\beta) = \frac{\Gamma(\alpha)\cdot\Gamma(\beta)}{\Gamma(\alpha+\beta)}, \qquad \Gamma(n) = (n-1)!, \tag{5.1}$$

where x is the variable in question (agglomerate area) and α and β are parameters that determine the appearance of the distribution function. Fitting the areas shown in the histogram gives $\alpha = 0.249$ and $\beta = 11.08$. In Figure 5.5c a uniform distribution is shown in orange and a beta distribution with the aforementioned parameters is shown in blue. These distributions can now be utilised in a polygon system generation script and will govern how randomised parameters are generated. Below the script is initialised.

```
[areas,xs,ys] = GetImageClusters(false); % Get data from scanned image
pd = fitdist(areas'/max(areas),'Beta'); % Fit areas to a beta distribution function

afrac = 0.38; % Desired area fraction
lowerbound = 0.07; % Sets a lower bound for agglomerate size
             % This is required due to some limitations in the Ansys software
```

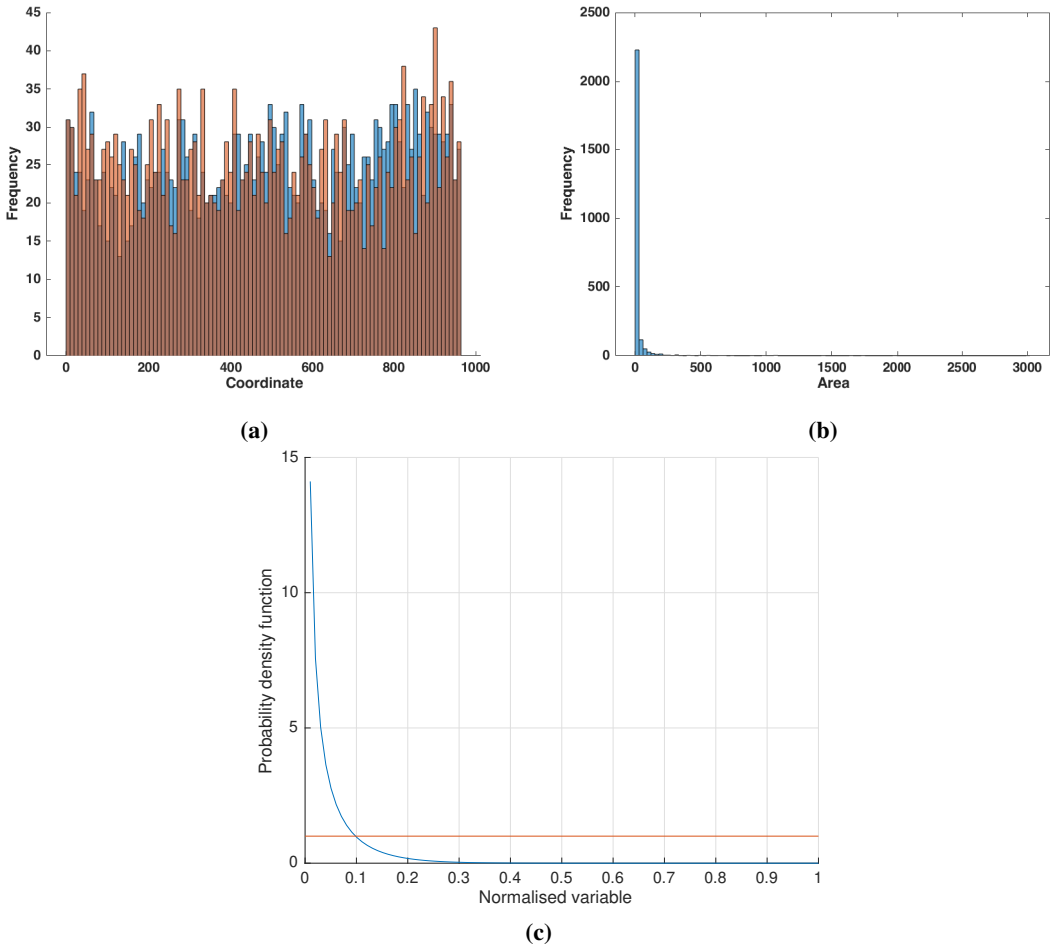

Fig. 5.5 Histogram of agglomerate coordinates and areas along with the corresponding fitted distribution functions.

```
verts = 5; % Vertices in agglomerate polygons
width = 10; % Width of composite system in mm
height = 10; % Height of composite system in mm
allpolygons = zeros(4,10000); % A matrix containing the line segments of all polygons
```

When polygons are generated and placed, they must not encroach on the area of another polygon, otherwise the model can not be solved in Ansys. This problem is solved by keeping track of which areas the placed polygons are occupying in a matrix, with a size according to an accuracy parameter. These concepts will be explained further later, but first the generation of a polygon is presented. The algorithm below will keep generating and placing polygons until the desired area fraction is reached.

```
occacc = 100; % Accuracy (resolution) of the occupation checking matrix
canmask = zeros(height*occacc,width*occacc); % Initialise occupation matrix
totarea = 0; % Total area of the placed polygons
curafrac = 0; % The accumulative volume fraction the placed polygons represent

while(curafrac<afrac) % Execute the following code as long as the accumulative area fraction is less than the
    desired
     randarea = random('Beta',pd.a,pd.b)*max(areas); % Get random area according to distribution function
     aveR = sqrt(randarea/pi) + lowerbound; % Convert the area to an average radius
     stencil = GeneratePolygon(verts,aveR,0.7,0); % Generate a polygon
     ww = round(max(stencil(1,:))*occacc); % Width of polygon
     hh = round(max(stencil(2,:))*occacc); % Height of polygon
```

Now the polygon has been created and it must be converted to a matrix containing ones and zeros, which

is done by the `poly2mask` function. In the created matrix, entries are one if they are part of the polygon and zero if otherwise. An example of such a mask is visualised in Figure 5.6, where the exact polygon have been discretised into matrices of different sizes, governed by the value of the accuracy parameter, `occacc`. Yellow squares represent entries in the matrix that are one, and blue squares represent entries equal to zero. By using a larger matrix for discretisation, edges can be represented more accurately, but more computation power is required for performing the discretisation. The algorithm below attempts to place the generated polygon into the canvas and will move it around until a free space has been encountered or over 100 attempts at placing it have been done. When a free space is found, the discretised mask is placed into a matrix that represents the mask of the entire canvas and thus contains all placed masks.

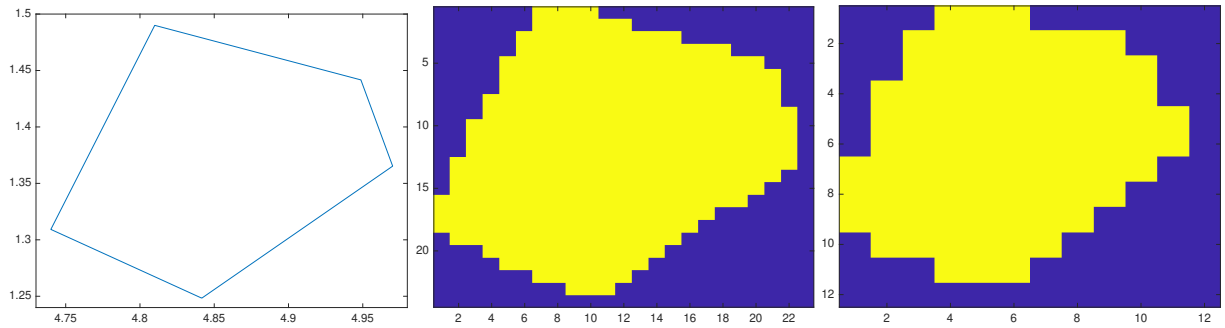

(a) **(b)** **(c)**

Fig. 5.6 An exact polygon to the left have been discretised into the matrices on the right. In the middle occacc = 100 and to the right occacc = 50.

```
        polmask = poly2mask(stencil(1,:)*occacc,stencil(2,:)*occacc,hh,ww); % Generate a mask
        canplace = false; % Initially the mask can not be placed
        n = 0; % Number of attempts that have been done to place the polygon
        while(~canplace)
            n = n + 1;
            if(n>100) % If placement attempts exceed 100, give up
                disp('Could not fit stencil in canvas')
                break;
            end
            shiftx = round(unifrnd(1,width*occacc)); % Generate a random number for placement in x
            shifty = round(unifrnd(1,height*occacc)); % Generate a random number for placement in y
            if(shifty+hh-1>length(occ(:,1))) break; end % Skip this attempt if the stencil would exceed
            if(shiftx+ww-1>length(occ(1,:))) break; end % the canvas boundaries

            check = canmask(shifty:shifty+hh-1,shiftx:shiftx+ww-1); % Get the checked region of the canvas mask
            add = check + polmask; % Add the stencil mask
            if(max(max(add))==1) % If the highest value in add is 1, the placed stencil does not encroach on an
                 already placed stencil
                canplace = true; % It is possible to place it
                canmask(shifty:shifty+hh-1,shiftx:shiftx+ww-1) = add; % Add the stencil to the canvas
                totarea = totarea + polyarea(stencil(1,:),stencil(2,:)); % Note the area of the added polygon
                % Update the coordinates of the polygon to be shifted
                stencil(1,:) = stencil(1,:) + shiftx/occacc;
                stencil(3,:) = stencil(3,:) + shiftx/occacc;
                stencil(2,:) = stencil(2,:) + shifty/occacc;
                stencil(4,:) = stencil(4,:) + shifty/occacc;

                % Insert the polygon into our list of polygons
                cola = (i-1)*length(stencil(1,:))+i;
                colb = cola+length(stencil(1,:))-1;
                allpolygons(1:4,cola:colb) = stencil;

                curafrac = totarea/(width*height); % Update the accumulative area fraction
            end
        end
    end

allpolygons(:,i*(verts+1)-verts:end) = []; % Trim the list of polygons
```

At this point all polygons should have been placed and the generated matrix of polygon coordinates can be written to a text file that can be parsed by Ansys software. Ansys require for there to be a header that specifies how the data should be interpreted. It is also required for coordinates of vertices belonging to a polygon to be separated by an empty line, taken care of by a simple loop as shown below

```
fID = fopen('polygons.txt','w');
% Setup a header
fprintf(fID,'%s\r\n','3d=true');
fprintf(fID,'%s\r\n','polyline=true');
fprintf(fID,'%s\r\n','fit=true');
% Write the points grouped into separate polygons
for i=1:length(allpolygons(1,:))
   w = allpolygons(:,i);
   if(w(1)==0 && w(2)==0 && w(3)==0)
      fprintf(fID, '%s\r\n','');
   else
      fprintf(fID, '%f %f %f %f\r\n',w);
   end
end
fclose(fID);
```

This file must then be read by Ansys, which is made possible by the use of software macros, that execute tasks normally available to the user only through a graphical user interface.

Converting a list of polygons to a CAD-model

Macros in Ansys are written in Python language, that have been conformed to their own application programming interface (API), so the syntax is different from the code presented so far. The file containing polygon coordinates is opened and each line in the document is extracted. In order to draw a CAD-model a sketch plane must be defined, which in this case is chosen to span the x-z axes. Then each document line in the opened file is iterated through and a line segment is drawn on the sketch plane according to the coordinates designated in the document. Ansys knows to connect lines at intersection points, so properly connected polygons are created.

```
fID = open('polygons.txt','r') # Open file
Lines = fID.readlines() # Extract lines

sectionPlane = Plane.Create(Frame.Create(Point.Create(MM(0), MM(0), MM(0)),
   Direction.DirX,
   Direction.DirZ)) # Define sketch plane

for line in Lines:
   if (line.find('=') != -1): # Do not draw line segments if the read line is a header
      continue
   if(line.find('.') != -1):
      x1,y1,x2,y2 = [float(i) for i in line.split()] # Get coordinates for two points
      p1 = Point2D.Create(MM(x1), MM(y1)) # Create a point
      p2 = Point2D.Create(MM(x2), MM(y2)) # Create another point
      SketchLine.Create(p1, p2) # Draw a line between the two points
```

From here the user can manually extrude the drawing in order to create a pseudo-3D area element, which can be imported in the material designer tool. However, due to the complexity of the geometries constructed the tool was not able to solve the systems drawn and thus find its corresponding material properties. This was an unexpected outcome, as the tool is practically built around generating pseudo-random volume elements containing hundreds of individual filler particles, where complicated features such as orientation and anisotropy of filler particles can be accounted for, even in three dimensions. It seems the custom geometry function, that was to be used in this work, is intended for the creation of simpler structures such as regularly ordered fiber mat composites and the like. So instead of using this tool as originally desired, the conventional finite element solver was utilised. Although less accurate, it would be possible to determine the effective stiffness of the volume element created by applying a force in a given direction, and using the average strain of the plane where the force is applied at, in the equation of Hooke's law ($\sigma = E\epsilon$).

An example of this is given here, where pristine PP with a known stiffness of $1350\,\mathrm{MPa}$ is subject to an applied force. A $5\,\mathrm{mm} \times 5\,\mathrm{mm} \times 1\,\mathrm{mm}$ block of PP seen on Figure 5.7 is subject to a force of $1000\,\mathrm{N}$ in the x-direction distributed evenly across one face, A, marked in red. The opposite face, B, has been fixed and the average strain of plane A in the x-direction subject to the applied force is found to be 0.149, which reveals a stiffness of $1341.8\,\mathrm{MPa}$, close to the actual stiffness. The size of elements, shown as a grid, have been carefully chosen to be half of the thickness of the block, so the block is not subject to strain in the y-direction. A small test was carried out to confirm this, were similar blocks with a thickness of 0.1 and $5\,\mathrm{mm}$ were subject to the same force and with a mesh configured appropriately. The calculated stiffness was 1341.4 and $1340.3\,\mathrm{MPa}$ respectively, showing that the strain in the y-direction effectively have little to no effect on the calculated stiffness when using this method.

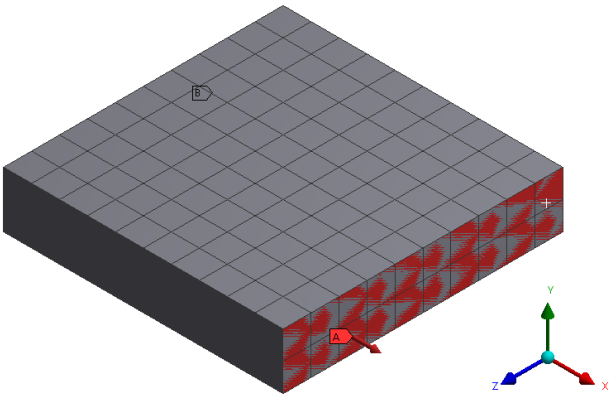

Fig. 5.7 PP block used in the example.

Chapter 6

Results and discussion

The outcomes of all experiments are presented in this chapter, along with an immediate interpretation of what is observed. These interpretations will be based on knowledge acquired from the experiments presented before the corresponding experiment and from what was found in the literature study.

6.1 Light-optical microscopy

Microscopy was utilised to evaluate the results of several experiments, namely the dispersion of GO in water following sonication and the evolution of agglomerates in a PVA/GO solution. It was also used to analyse the degree of agglomeration observed in the produced PP tensile test specimens, presented firstly.

Polypropylene composites

The primary objective for the functionalisation procedure, was to influence the degree of agglomeration in the PP composites. This parameter is assessed using optical microscopy on thin slices of tensile specimens, acquired by sanding and polishing. Samples of either composite had a thickness of around $230\,\mu\mathrm{m}$ and were inspected using transmissive light microscopy at 5X magnification. In order to obtain information about the degree of agglomeration, a large area was captured in the microscope, by stitching together multiple images. Completed images were then color corrected so filler particles are completely black and clearly distinguishable from the surrounding translucent plastic. Agglomerate characteristics were acquired using the script described in Section 5.2, where the size and location of each particle could be found, however in this case only their size are interest. The obtained images can be seen on Figure 6.1, where the analysed area is encompassed by a red square, and identified particles have been highlighted in red. The specimens shown have a width of $12\,\mathrm{mm}$.

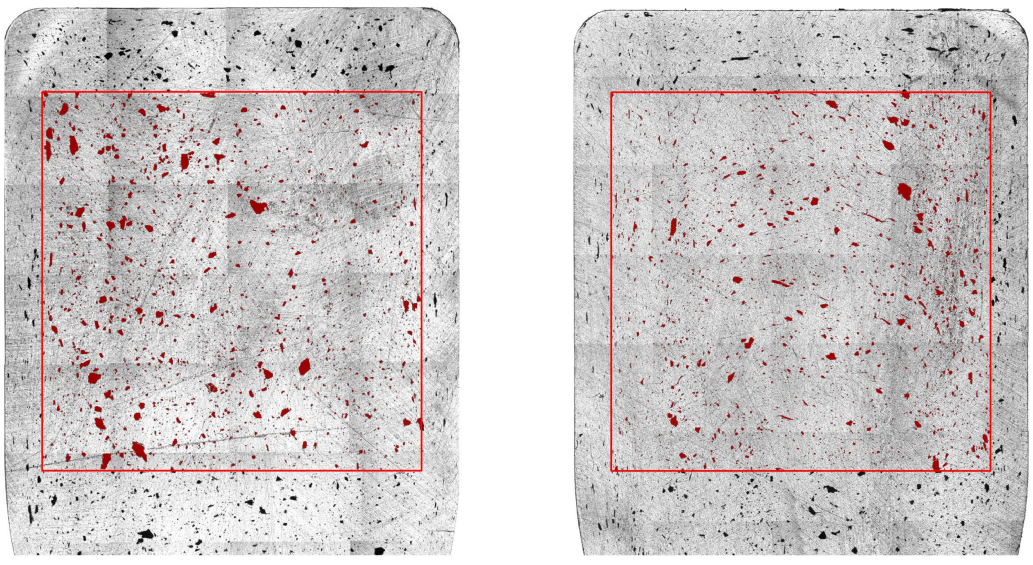

(a) **(b)**

Fig. 6.1 LOM images of PP composites at 5X magnification. To the left is the composite containing GO and to the right is the composite containing NaOH-GO.

A composite of optimally dispersed filler would not have any visible particulates, but instead the plastic would have attained a discoloration, as was seen with PVA in the preliminary experiments. In the given case, particles are easily distinguishable, which is evident of poor dispersion, but smaller particles are generally preferred over larger ones. Following the compounding of composite material it was noted how much material had actually been added to the composites, and these values are shown in Table 6.1. The filler contents are not the same, which is also evident when counting particles and calculating the percentage of area covered by filler on the images captured. This might make the specimens incomparable, as a composite with a higher concentration of filler is more likely to have agglomerates formed. For now it is assumed the discrepancy is small enough to be insignificant. The mean particle size (area) have been found for both composites, and it seems a reduction in particle size have followed the functionalisation procedure. However, both data sets have high standard deviations, which is a result of the abundance of small specs of filler material, that have areas of a single pixel, while there are only a couple larger agglomerates. This can be easily recognised when plotting the histogram of the areas, seen on Figure 6.2

	PP-GO	PP-NaOH-GO
Filler content [wt%]	0.57	0.43
Filler content [area%]	5.2	3.7
Particle count [-]	3213	2787
Mean area [μm^2]	1612	1325
σ [μm^2]	5632	4108
Δ area [μm^2]	103775	110007

Tab. 6.1 Particle properties as observed in the two composites.

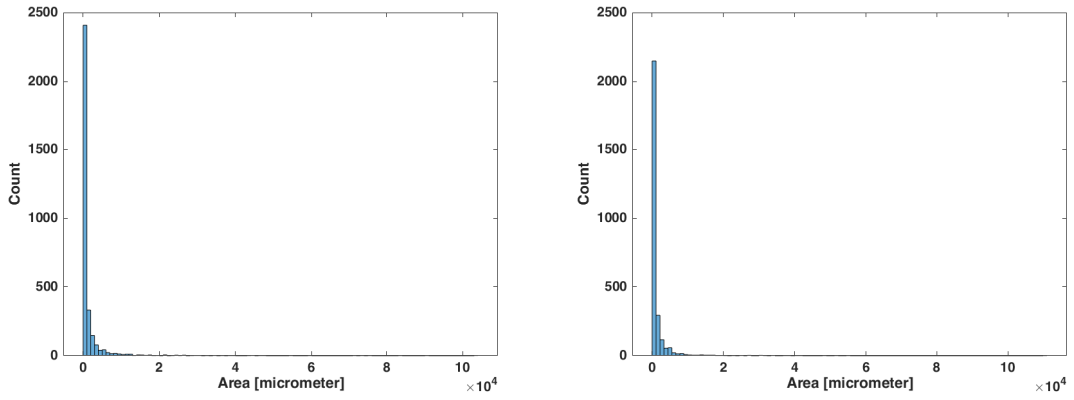

Fig. 6.2 Histogram of area distributions of PP composites with (a): pristine graphene oxide, (b): base-catalysed functionalised graphene oxide.

There is a large concentration of smaller particles for both samples, and a sharp drop in concentration of particles of other sizes. Only a few particles have areas above $2 \times 10^4\,\mu m^2$, which make up the larger particles, easily visible on the microscopy images. The difference between the largest and smallest particle (Δarea) of either composite is also similar, again showing evidence of no change in degree of dispersion of particles following the functionalisation procedure. The data acquired is generally quite difficult to conclude

on, due to the high variances seen, but the overall tendency seems to be that no change in agglomeration have occurred after particles have beeen functionalised.

Sonication

The sonication procedure is thought to break up agglomerates, so it is interesting to note their size distribution following such a treatment. Microsocopy images of the water/GO suspensions can be seen on Figure 6.3, all of which were acquired immediately after sonication. The solution temperature was also probed immediately after sonication, and showed both of the 20% (sonication intensity) tests were around $70\,^{\circ}\mathrm{C}$, and both of the 60% tests were around $75\,^{\circ}\mathrm{C}$, so it seems the solution temperature depends mostly on the sonication intensity and less on the time. Most of the images seem to have similar degrees of dispersion, so in order to distinguish more clearly between them, particles were identified and counted like in the previous section, providing information about their sizes as presented in Table 6.2.

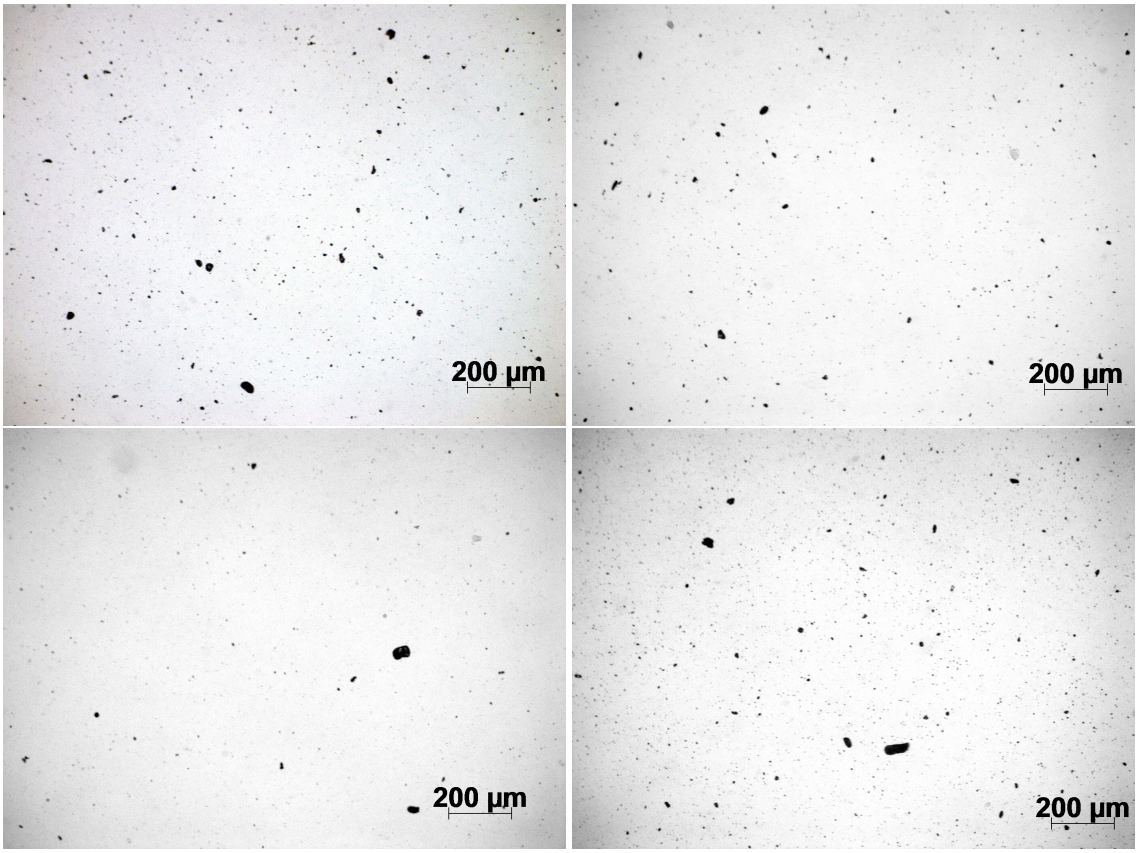

Fig. 6.3 Transmissive LOM images of graphene/water suspensions at 10X magnification. From upper left going clockwise: 10min-20%, 10min-60%, 50min-60%, 50min-20%.

When sonicated for $10\,\mathrm{min}$, the largest particle had an area of around $400\,\mu\mathrm{m}^2$, while samples sonicated for $50\,\mathrm{min}$ had particles with an area of up to $1500\,\mu\mathrm{m}^2$. Prolonged sonication might be causing particles to reaggregate, possibly due to oxide moieties being reduced as a result of excessive heating over a longer period of time. The difference in temperature of $5\,^{\circ}\mathrm{C}$ is not thought to be significant enough to produce this variance, the difference in time of $40\,\mathrm{min}$ seems to be a more likely culprit. Additionally, histograms (shown on Figure 6.4) of $10\,\mathrm{min}$ samples have several particles with close to minimal size, as in the distribution has a taper from 0 to $100\,\mu\mathrm{m}^2$. Histograms for the $50\,\mathrm{min}$ practically only contain incredibly small particles and

	10min-20%	10min-60%	50min-20%	50min-60%
Particle count [-]	518	276	132	790
Total area [μm^2]	14142	8639	4946	17800
Mean [μm^2]	27.30	31.30	37.47	22.53
σ [μm^2]	69.62	91.28	184.9	151.7

Tab. 6.2 Particle properties determined from the LOM images captured.

a few larger particles. This suggests the extra sonication time is efficient for breaking up agglomerates and that sonication intensity is less important. The amount and total area of particles present in the sample seem to be varying wildly, and there is no clear relation between sonication time or intensity, and the amount or total area of particles. The variations seen can be a result of local differences in particle concentration in the liquid deposited on the watch-glass. There does not seem to be a clear relation between sonication parameter and mean size of particles and this is further complicated by the large variances in particle size. It seems the overall particle size, and therefore dispersion quality, is indifferent to the sonication parameters investigated, however it should be stressed the results are not deemed definitive, and that more work regarding this topic should be carried out.

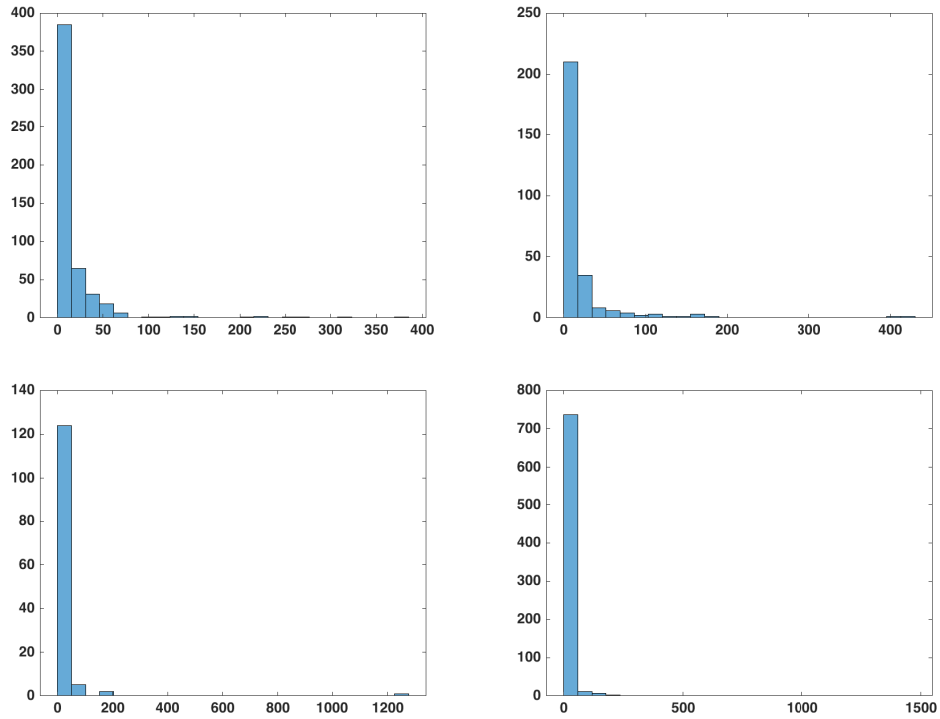

Fig. 6.4 Histogram of particle area in μm^2. From upper left going clockwise: 10min-20%, 10min-60%, 50min-60%, 50min-20%.

6.2 Agglomeration timelapse

This section involves the study of the mechanism of agglomeration in PVA composites, done through a timelapse. The timelapse proved less trivial than expected, as the particles in the solution would constantly move out of focus, requiring for occasional manual re-focusing of the image. This is evident on the first pictures showed on Figure 6.5, taken at 10X magnification, meaning images are around $7\,\mathrm{mm} \times 5\,\mathrm{mm}$. To the left the first image can be seen, taken immediately after the solution was deposited on the watch-glass. Several relatively large particles are already visible even before the solution has been allowed to settle. With time, these particles sunk down (into the page) in the liquid and the clearly visible particles moved out of focus, and some other particles are instead visible on the image to the right. It is thought the particles observed on the leftmost image was floating near the surface of the liquid and slowly moved towards the surface of the glass substrate. In the meantime smaller particles freely float around in the liquid by convection caused by the evaporation of water.

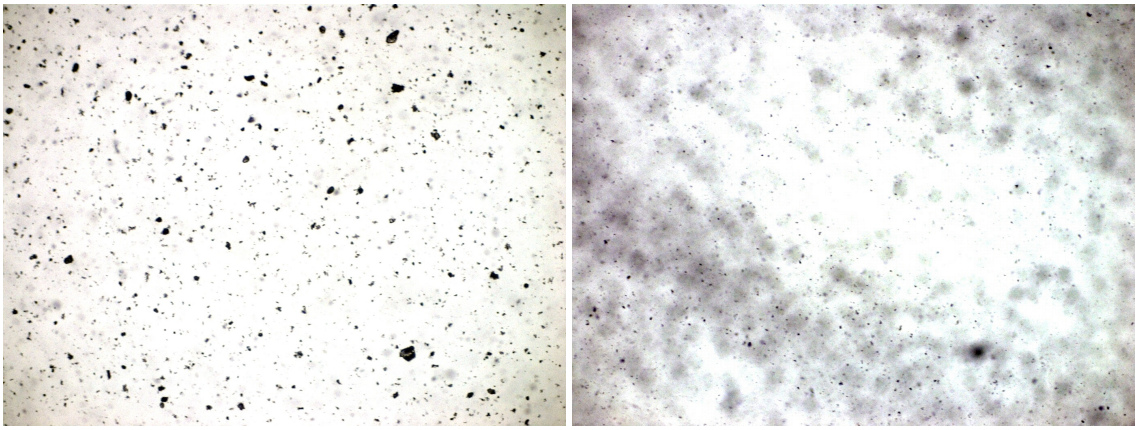

Fig. 6.5 Solution at 10X magnification. Left: $0\,\mathrm{min}$, right: $111\,\mathrm{min}$

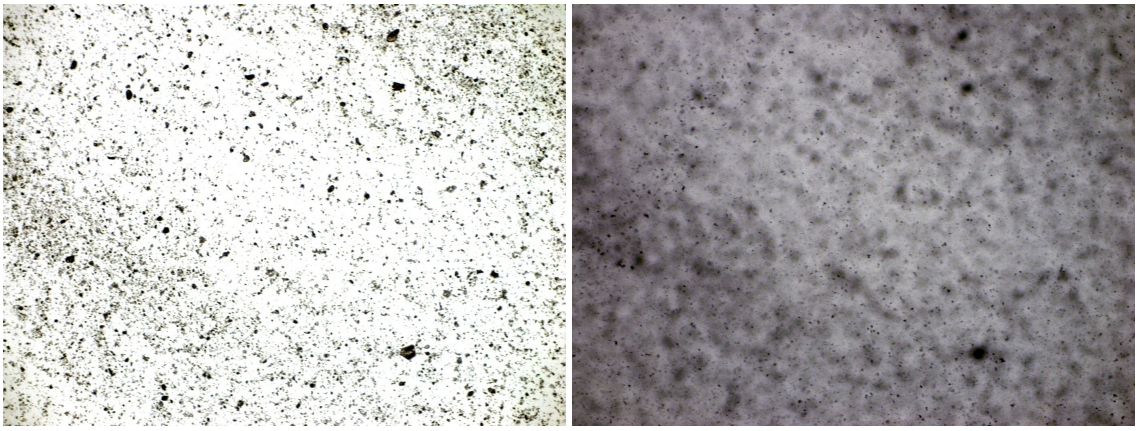

Fig. 6.6 Solution at 10X magnification. Left: $132\,\mathrm{min}$, right: $300\,\mathrm{min}$

The initially observed particles were moved back into focus about two hours into the experiment seen to the left on Figure 6.6. Compared to the first image taken, small particles have appeared, swept across the surface, thought to have settled from the bulk solution. It is interesting only additional small particles have appeared, suggesting only they are able to move around laterally in the fluid, while larger particles are confined to only move from the pull of gravity. During the next two hours, the image gradually gained a

dark tint and got out of focus again, as can be seen on the image to the right. This is thought to be a local high concentration front of particles sweeping across the surface, as will be evident in the next image. To the left on Figure 6.7, the edge of the concentration front can be seen as it moves upwards across the surface, which occurred over the course of about twenty minutes. This is an interesting phenomenon, and could be explained by the evaporation of water in the solution. The water does not evaporate evenly across the surface of the watch-glass, so when a point eventually becomes completely dried out, a wet/dry interface appears. This is the interface that is clearly visible to the left on Figure 6.7. The dark tinting is thought to appear as particles close to the interface is pushed in the same direction the interface is moving, increasing the concentration of particles locally. When the interface sweeps across the surface, some particles are also left behind, which become part of the dried plastic. After the interface had disappeared from the image, the image seen to the right was observed, and remained unchanged for the next several hours. So it is evident the plastic is completely dry at this point.

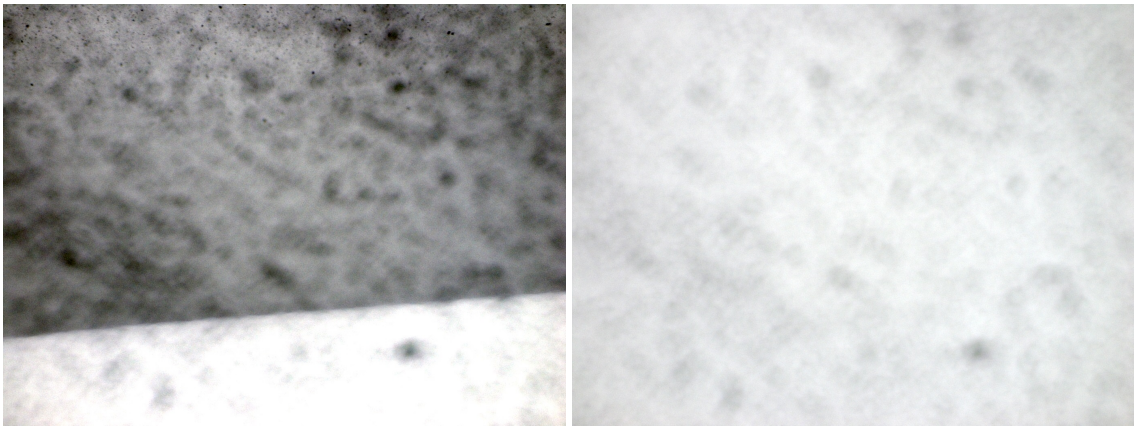

Fig. 6.7 Solution at 10X magnification. Left: $320\,\mathrm{min}$, right: $520\,\mathrm{min}$

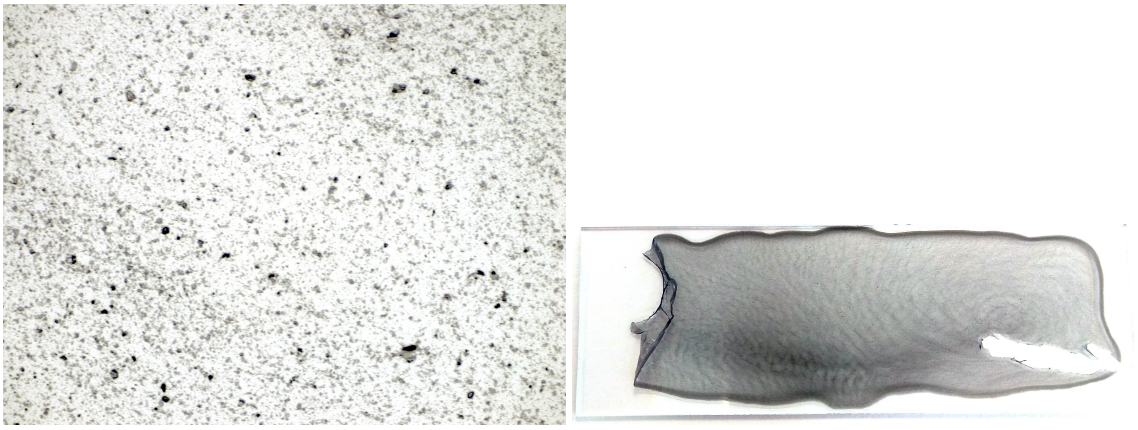

Fig. 6.8 Left: Solution at 10X magnification $1313\,\mathrm{min}$ into the test. Right: completely dried film.

The experiment was halted prematurely due to this fact, and a final in-focus image was captured as shown to the left in Figure 6.8. To the right is a macroscopic picture of the film acquired from the experiment where the variances in filler concentration can be seen clearly. In particular is the high concentration around the edge of the film, thought to be stemming from the front that had been moving across the surface previously.

In conclusion it seems the larger particles settle in the fluid almost immediately, while smaller particles are fairly mobile. Convection forces, formed due to the evaporation of water, acting on the particles are

not high enough to affect the larger particles. Particle mobility could also be inhibited by polymer chains present around the particle, which smaller particles can move between more easily. By inspecting the general size of the particles that have appeared in the final image, that were not present on the first image, this threshold size could be determined. No formation of agglomerates were observed per se, only the settling of existing particles could be seen. Some small particles are settling onto larger particles, effectively forming agglomerates, but does not seem to be preferring to do so. So either agglomeration occur at a much smaller scale, or the particles visible have a size determined by previous processing steps, i.e. sonication or exfoliation. This hints at the fact that the agglomerates observed are in fact graphite that has not been exfoliated properly.

6.3 Tensile

Tensile tests were performed on composites of PP and PVA, where the former consisted of three types: pristine (PP), with pristine GO (PP-GO), and with base-catalysed functionalised GO (PP-NaOH-GO, while the latter consisted of two types: pristine (PVA) and with pristine GO (PVA-GO). Tensile curves for the PP composites can be seen on Figure 6.9 and determined mechanical properties are shown in Table 6.3. Specimens of pristine PP had tensile curves of consistent appearance with ultimate tensile strengths of around $34\,\mathrm{MPa}$, necking at around $4\text{-}5\,\mathrm{mm}$ and with no fracture occurring for the applied displacement. According to the datasheet provided by the supplier, the polymer should have a stiffness of $1350\,\mathrm{MPa}$, which is considerably lower than what is measured in the performed tests. The ultimate tensile strength should also be $32\,\mathrm{MPa}$, which is higher in the tested case. This is attributed to degradation of the polymer by ultraviolet radiation during storage. Cross-linking of polymer chains occur as a result of this, which effectively lead to an embrittlement of the material. Its deviation from the datasheet is not of concern in the given case, as the acquired data only acts as a control for the other series presented. Specimens of PP composites containing pristine graphene oxide were tested next, and the measured tensile curves can be seen in Figure 6.9b.

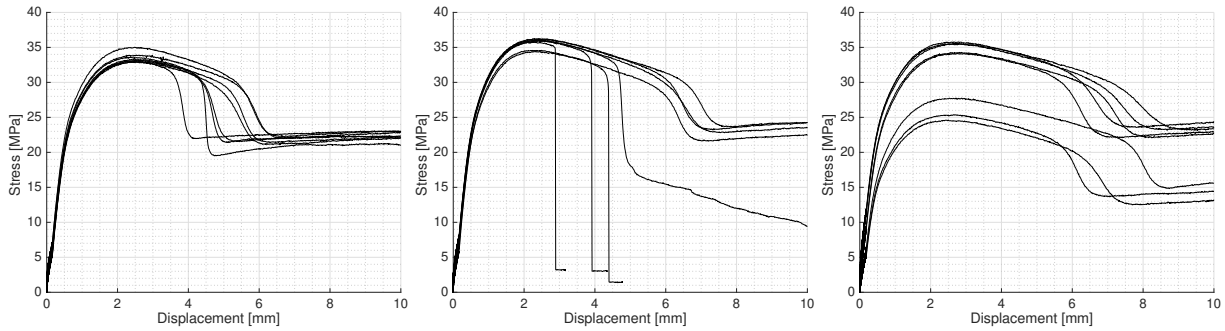

Fig. 6.9 Tensile curves for PP specimens where (a) pristine PP, (b) graphene oxide in PP, (c) base-catalysed functionalised graphene oxide in PP

A minor increase in stiffness, ultimate tensile strength and strain at necking is observed, but specimens have attained a less consistent behaviour being either relatively brittle or ductile. The stronger ductile type practically behaves the same as the control, but exhibits the aforementioned strengthened properties, while the brittle type (specimens no. 1, 3, 4, and 7) experienced premature necking, often resulting in fracture. This is attributed to the GO having poor interphasial adhesion to the surrounding polymer effectively acting as a void in the material, thus leading to sites of stress concentration where cracks tend to form at reduced applied stresses. The inconsistencies observed are a result of the stochastic nature of the distribution and

	Specimen no.	1	2	3	4	5	6	7	8	Mean	σ
PP	E	1730	1880	1780	1790	1730	1670	1770	1800	1769	61.75
	σ_{ut}	33.9	35.0	33.6	33.3	33.0	33.0	33.2	33.0	33.5	0.69
PP-GO	E	1850	1860	1870	1910	1840	1890	1870	1920	1876	28.25
	σ_{ut}	34.6	34.4	36.1	35.8	36.3	36.2	36.0	36.0	33.7	0.74
PP-NaOH-GO	E	2460	3210	3220	1960	2020	3110	3330	3200	2814	574.4
	σ_{ut}	27.7	34.2	34.3	24.6	25.4	35.6	35.8	35.5	31.6	4.86

Tab. 6.3 Mechanical properties of PP composites in MPa

size of particles, meaning it is practically coincidental if the placement and size of a given particle will cause premature fracture or not, thus leading to the inconsistent tendencies observed. Overall the results hint at the strength-enhancing properties, graphene can have on a polymer, provided a given specimen is behaving optimally without premature fracture. Finally the composites containing base-catalysed functionalised graphene oxide were tested and the results can be seen on Figure 6.9c. Most noticeably is their high stiffness of around $2800\,\mathrm{MPa}$, which is a considerable increase of around 60%, as compared to the pristine material. This is evidence of the particles interacting properly with the surrounding polymer, meaning load is transferred to the particles and the composite has begun to exhibit the properties of the graphene. Ideally this is the result of the attached non-polar stearic acid chains having an appreciable affinity for the polymer, as opposed to the polar nature of prsitine graphene oxide, which detest the polymer. These specimens exhibit necking at around 6-$8\,\mathrm{mm}$ displacement, which is a minor improvement compared to the previous series. Inconsistencies across specimens are also observed, also grouped like for the pristine graphene oxide, but now also with considerable differences in mechanical properties. Three specimens (no. 1,4, and 5) have lower ultimate tensile strengths and stiffnesses than the rest of the specimens in the series, but with a similar strain at necking. Although it is not surprising there are variances in the data cf. what was seen in the previous series, the particular grouping of tensile curves and corresponding mechanical properties is interesting. These three specimens all have both lower ultimate tensile strength and stiffness, which was not the case in the previous series. A possible, albeit unlikely, explanation for this could be differences in filler content that could have incurred during moulding, as specimens were moulded in batches of two or three. Conclusively, the base-catalysed functionalisation procedure employed was mildly successful at enhancing the mechanical properties of the polymer, although some irregularities were still apparent in the specimens. However, the strengthening effects observed going from pristine to functionalised GO can *not* be attributed to the change in agglomeration degree, as it was practically the same for both. This suggests other effects are causing the increases in stiffness, which might be stemming from increased crystallinity or stronger interphasial bonding.

Tensile tests performed on PVA specimens showed a markedly different material, as seen on Figure 6.10a, where no easily distinguishable elastic region could be identified, meaning the stiffness of the material had to be determined manually. Manual determination of the stiffness was done by identifying a linear region of stress-strain on the tensile curve and finding the slope of said linear region. Resulting stiffnesses can be seen in Table 6.4. Pristine PVA specimens show a tensile curve akin to that of rubber, where stress is steadily increasing with applied strain until rupture occurs instantaneously. The material exhibited a low stiffness of around $38\,\mathrm{MPa}$, although with a high variance, stemming from the irregularity in specimen appearance. Specimens were crumbled and warped as a result of the drying process, and contained varying concentrations of bubbles, both altering the properties of the specimen. Additionally, the strain was only measured using the movement of the crosshead, as opposed to using an extensometer,

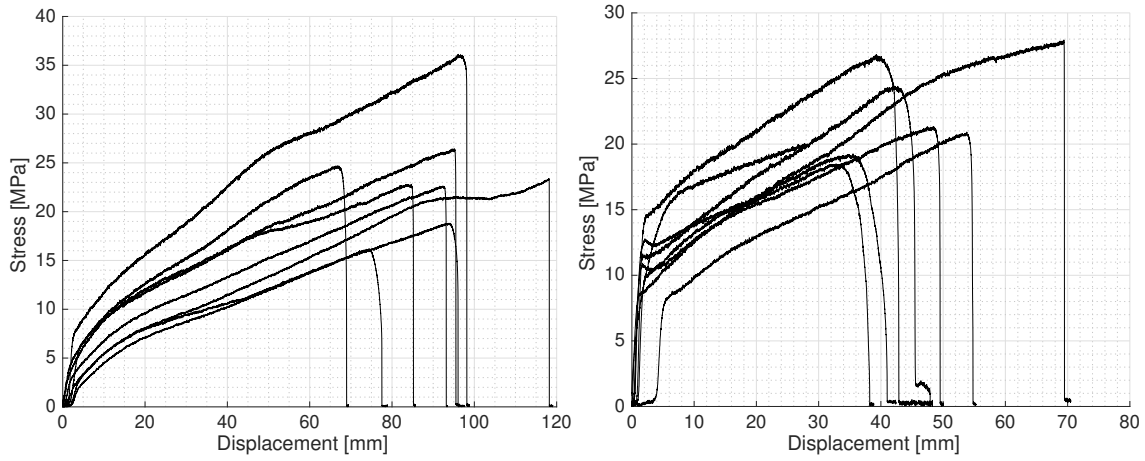

Fig. 6.10 Tensile curves for PVA specimens where (a) pristine PVA, (b) pristine graphene oxide in PVA

		1	2	3	4	5	6	7	8	Mean	σ
PVA	E	32.68	33.44	8.731	30.60	12.10	128.0	18.42	42.47	38.31	38.05
	σ_{ut}	24.70	26.45	18.81	22.61	23.37	36.12	16.20	22.81	23.88	5.91
	t	310	325	445	405	460	260	495	365	383	76.6
PVA-GO	E	-	235.8	109.9	180.8	215.3	197.5	247.1	239.9	203.8	47.82
	σ_{ut}	-	27.77	20.92	19.24	24.45	21.33	26.83	18.52	22.72	3.66
	t	-	290	320	290	245	315	225	300	281	32.9

Tab. 6.4 Mechanical properties of PVA composites in MPa and $\mu\mathrm{m}$.

which is not considered accurate for determination of stiffness. The low stiffness is not surprising though, as the type of polymer used is easily stretched even without the aid of machinery. There seemed to be no relation between ultimate tensile strength and thickness, although otherwise expected. Specimens did not have constant cross-sectional area and the ultimate tensile strength exhibited is probably a result of the thickness of the thinnest cross-section, which was not measured. Specimens containing pristine GO also behaved rubbery, although a distinctive elastic region had appeared, as seen on Figure 6.10b. Stiffnesses were again determined manually due to the variance in curve appearance. It should also be noted that a specimen was omitted from the data set, as it was subject to a machine error during testing. A drastic five-fold increase in stiffness was observed following the addition of GO, which could be indicating a high degree of polymer-filler interaction. GO is a polar material, as is PVA, so the two have a naturally high affinity for each other, ensuring a high degree of load transfer. As a result the filler is able to carry a substantial amount of the applied stress, effectively increasing the stiffness of the composite. Unfortunately it is not possible to compare the ultimate tensile stress of the two series, because it is not known if the specimens had similar cross-sectional areas, which is a critical factor in regards to strength. Still it can be concluded that GO had a substantial effect on the mechanical properties of the PVA, simply by the appearance of the measured tensile curves.

When comparing the tests of either matrix material, it is evident what magnitude of an effect a graphene filler can impart on a polymer material. The substantial increase in stiffness observed in the PVA/GO composite eludes to the fact that either low degrees of agglomeration and strong interphasial adhesion (or both) is critical when an increase in stiffness is desired. It can be suggested that these effects have

not fully been harnessed in the PP composites, but the functionalisation procedure did aid the process. Furthermore, GO did not seem to influence the ultimate tensile strength of the composite, it is included in, in any appreciable way, although it is difficult to conclude based on the results of the PVA composites.

6.4 Infrared spectroscopy

GO was inspected using infrared spectroscopy, even though it proved rather difficult to obtain useful spectra due to its high absorbance across the entire spectrum. The primary aim for the analysis was to identify the peaks belonging to the oxide groups on GO and determining if the substance had in fact been functionalised by the employed functionalisation procedure. Attempts were made at suspending the GO in either ethanol or water, covering an ATR-crystal with the suspension, and by subtracting the IR-spectrum of ethanol or water accordingly, a spectrum for GO would be acquired. However, since both solvents contain an abundance of either hydroxyl or C-H groups, as does both pristine and functionalised GO, it was not possible to discern which peaks belonged to the solute or the corresponding solvent. Instead the suspension was deposited on a mica disk and left to dry, leaving behind a GO-covered substrate that could be analysed using a probe ATR-crystal. Obtained spectra are presented in black and each have been baseline corrected according to the red line directly below the spectrum, and then deconvoluted to obtain the spectrum seen in green, where identified peaks are also shown in red. The baseline shown in all spectra are probably overcompensating, but it has been placed in order to allow for the fitting software (Fityk v. 1.3.1) to automatically identify peaks that are already visible from the uncorrected spectrum. As a result of this overcompensation, some artefacts are thought to have appeared during peak deconvolution, which are disregarded of if they seem too indistinct on the original spectrum.

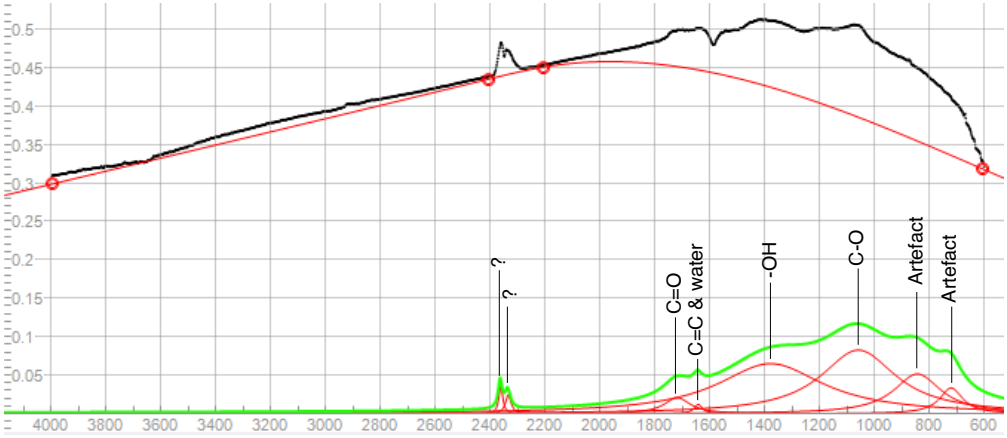

Fig. 6.11 IR spectrum of graphene oxide on mica.

Looking at the spectrum for pristine GO on Fig. 6.11, some peaks can be disregarded of. Bands at $720\,\mathrm{cm}^{-1}$ and $843\,\mathrm{cm}^{-1}$ are thought to be artefacts from the fitting procedure, as they are practically unidentifiable on the uncorrected spectrum, and no equivalent peaks could be found in the literature. All other peaks are distinctly visible on the uncorrected spectrum, and almost all could be characterised accordingly. The band at $1058\,\mathrm{cm}^{-1}$ is attributed to C-O stretching and specifically that of epoxide groups[72–74]. At $1378\,\mathrm{cm}^{-1}$ there is a broader peak belonging to the deformation vibration of hydroxyl groups[72,74–77] either directly attached to the graphene or belonging to carboxyl groups. A small peak can be seen at $1641\,\mathrm{cm}^{-1}$ and belongs to the graphitic C=C stretching and adsorbed water[69,72,74,77], but it is not possible to determine the concentration of either. The band at $1718\,\mathrm{cm}^{-1}$ appears due to the C=O stretching of carboxyl moieties[72,75,76,78]. The last two peaks at $2361\,\mathrm{cm}^{-1}$ and $2334\,\mathrm{cm}^{-1}$ were not possible to identify. In the

spectrum shown, a high contact pressure between crystal and sample, was applied. When using a low contact pressure these two peaks were only partially visible meaning they could possibly belong to some adsorbed substances. No substances used in the processing of the GO has peaks appearing in this region (spectra for sulfuric acid, mica, ethanol, water, (3-aminopropyl)trimethoxysilane, and stearic acid were checked), and might appear due to contaminants, unaccounted-for hydrogen bonds or drastic changes in frequency of vibration for existing bonds. Interestingly, no broad peak was observed around 3500-3200 cm^{-1}, which is typically observed in GO samples, belonging to hydroxyl groups thought to be abundant on the graphene surface. Its absence can suggest a low degree of general oxidation or the peak may be hidden due to the high absorbance in the entire spectrum.

On Fig. 6.12 a spectrum for GO functionalised *without* a base catalyst (prepared from previous work[1]) can be seen. Some similar peaks can be identified: C-O at 1091 cm^{-1}, as well as undesignated bands at 2335 cm^{-1} and 2363 cm^{-1}. However, the two bands previously seen around 1700 cm^{-1} have merged into a single peak and it can be suggested the visible peak belongs to C=O stretching. It is likely that previously sp^2 hybridised C=C bonds have been converted to sp^3 hybridised carbon bonds, which is supported by the appearance of two new bonds, at 2856 cm^{-1} and 2922 cm^{-1}, which belong to stretching of sp^3 hybridised C-H bonds[79], also commonly seen in alkyl chains. Whether the converted carbons now have hydrogen or oxygen moities attached is not clear from the spectrum. It is possible the C-H bonds belong to the alkyl chains in stearic acid, which is also suggested by the appearance of an additional broad peak at 3257 cm^{-1}[79], belonging to hydroxyl groups. Both hydroxyl and C=O moieties are present in stearic acid and from this it seems the graphene have in fact been functionalised, because no other source could supply the additional hydroxyl groups.

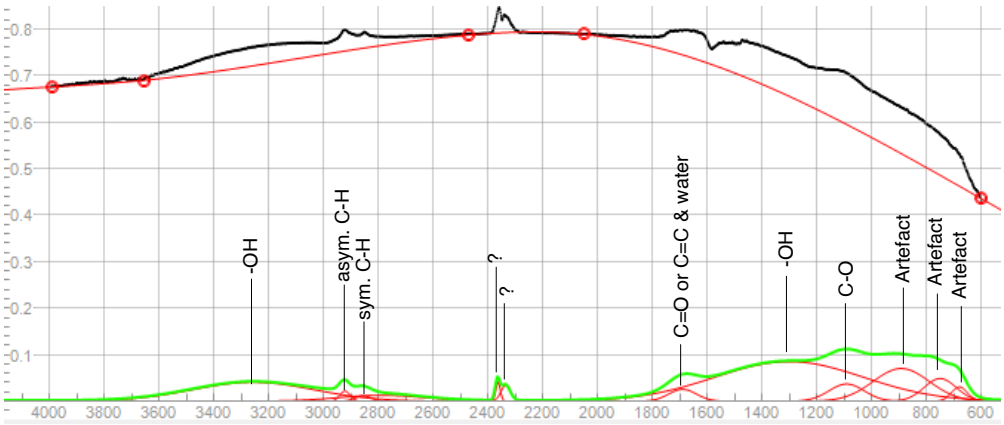

Fig. 6.12 IR spectrum of functionalised graphene oxide on mica.

The spectrum of the base-catalysed functionalised GO can be seen on Figure 6.13. Identified peaks are more noticeable as compared with the previous spectrum which is attributed to the lower overall absorption, meaning peaks are not as obscured. As for the previous spectrum, peaks at 1058 cm^{-1} and 1355 cm^{-1} belonging to C-O and hydroxyl groups can be seen. Contrary to the previous spectrum, peaks of C=C and C=O stretching have appeared again, this time at 1627 cm^{-1} and 1657 cm^{-1}, respectively. Their reapparance is thought to be solely due to this spectrum having lower overall absorption, making peaks more easily discernible. By this token it is evident there is still some unfunctionalisated carbon atoms on the graphene surface. Stearic acid still seem to be present, indicated by the peaks of C-H bonds at 2844 cm^{-1} and 2916 cm^{-1}, along with a peak of hydroxyl groups at 3381 cm^{-1}. Unlike the previous spectra, the uncharacterised peaks around 2300 cm^{-1} can not be seen on this spectrum, although some disturbances can be seen in this region on the uncorrected spectrum, meaning the substances they belong to are probably still

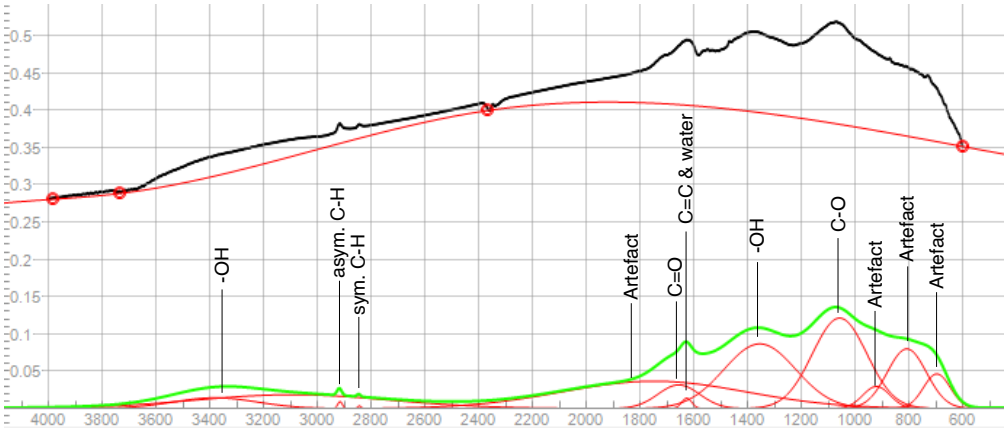

Fig. 6.13 IR spectrum of base-catalysed functionalised graphene oxide on mica.

present in this sample.

In general there seem to be no distinct differences between the spectra of GO functionalised by the two methods, and might suggest the base-catalysed reaction to be as effective as the unfunctionalised variant. However this is based on the supposition that either sample is completely free of adsorbed stearic acid, which might be present should the rinsing procedure have been inefficient. As such it is difficult to conclude definitively on which procedure is most effective or if the functionalisation reaction took place at all, although in conjunction with the results from tensile tests it could be said a chemical attachment have in fact occurred.

6.5 Model

The objective of this model was to represent the composites produced, by imitating their differences in agglomeration and studying how it changed their mechanical properties. However, as was observed in microscopy observations, no appreciable change in agglomeration had occurred following functionalisation. This means it was not possible to study the effects of agglomeration in experiments, since it did not change, and will therefore be investigated using the model presented here. So instead of basing the parameters used in the model on the actual specimens, the size distribution of agglomerates will be varied manually, in order to say something about what effect agglomeration *could* have had on the composites produced. The primary parameters to tweak with regards to agglomerate size distribution, are the parameters in the beta distribution functions, α and β along with the scaling of the function. When a number is generated using the functions, it lies somewhere between 0 and 1, and must then be scaled according to the size of agglomerates, and this scaling can be varied. Four analyses are carried out using two distribution functions and two different scalings. The distribution functions are varied so as to have either an abundance of small particles, or an abundance of large particles. These functions have been visualised respectively on Figure 6.14.

The scale of agglomerates will be chosen according to what is computationally practical, so that the composite with the smallest agglomerates, and therefore also with the most, can still be solved in a reasonable amount of time. More agglomerates make the model more complicated, which takes more time to solve. Agglomerates are scaled by multiplying a scale factor with the `randarea` variable in the script presented earlier and this factor is chosen to be either 0.1 or 1, meaning there will generally be a factor 10 in difference between the smallest and largest agglomerate created. Since the model is no longer representing the material system shown earlier, an arbitrary area fraction of agglomerates may be chosen. The value have been chosen in this case to be 0.2, as it strikes a good balance between creating enough agglomerates that

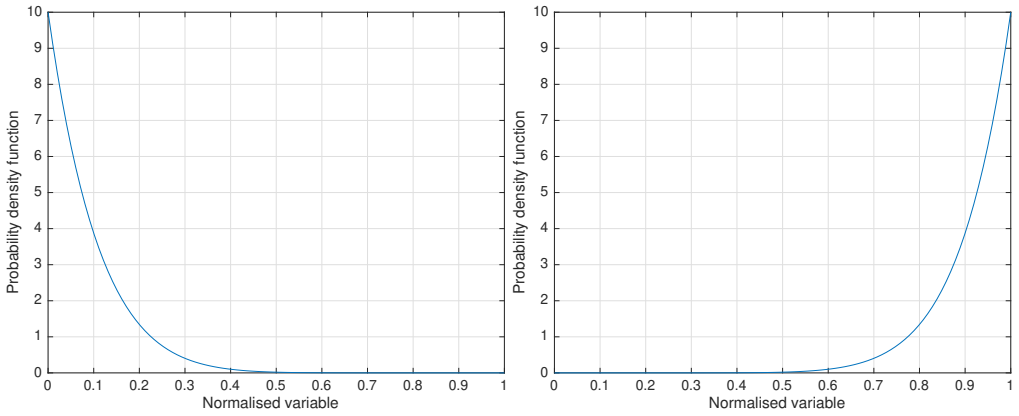

(a) **(b)**

Fig. 6.14 Beta distribution functions with varying parameters. (a): α = 1, β = 10. (b): α = 10, β = 1.

may influence the matrix, without creating too many, that complicates the model unnecessarily. Polygons of five vertices were chosen as the shape to represent the agglomerates, with `irr` and `spike` set to 0.7 and 0, respectively. Again these parameters can be chosen arbitrarily, but the particular parameters chosen produced shapes that looked somewhat similar to the agglomerates observed in microscopy, without becoming too complicated. In the tests done here, the agglomerates are assumed perfectly bonded to the surrounding matrix, although this is not the case in the actual composites. Agglomerates are given an isotropic stiffness of $1000\,\mathrm{GPa}$, which is the most typically determined stiffness for graphene as suggested by the literature, and the surrounding matrix is given an isotropic stiffness of $1350\,\mathrm{MPa}$, akin to the PP used in the experiments. Although graphene is not isotropic, directional effects are omitted completely in this model, so agglomerates are effectively oriented completely flat, which is practically the best case scenario for a two-dimensional material system. With the parameters presented, four composite systems are drawn as shown in Figure 6.15, designated according to Table 6.5.

Composite	(a)	(b)	(c)	(d)
α	10	10	1	1
β	1	1	10	10
Scale	1	0.1	1	0.1
Agglomerates	6	39	38	151
Mean area [mm^2]	0.8445	0.1288	0.1339	0.0332
σ [mm^2]	0.091	0.0125	0.0892	0.0142
Δ-area [mm^2]	0.2384	0.0641	0.4414	0.0687
Stiffness (average) [MPa]	1295	1354	1356	1380

Tab. 6.5

Based on the properties presented in the table, composite (b) and (c) are similar, having close to the same mean area and amount of agglomerates, but with different Δ-area (difference between largest and smallest agglomerate). This is exactly as would be expected, as the parameters for both (b) and (c) give agglomerates with areas on the order of $0.1\,\mathrm{mm}^2$, due to the appearance of either beta distribution and the scaling factor used. Other than that, the four composites have distinct agglomeration characteristics that reflect situations that might be observed in actual composites. The stiffnesses found for the simulated composites are also shown in Table 6.5. These numbers seem consistent with what is suggested by the literature, where better

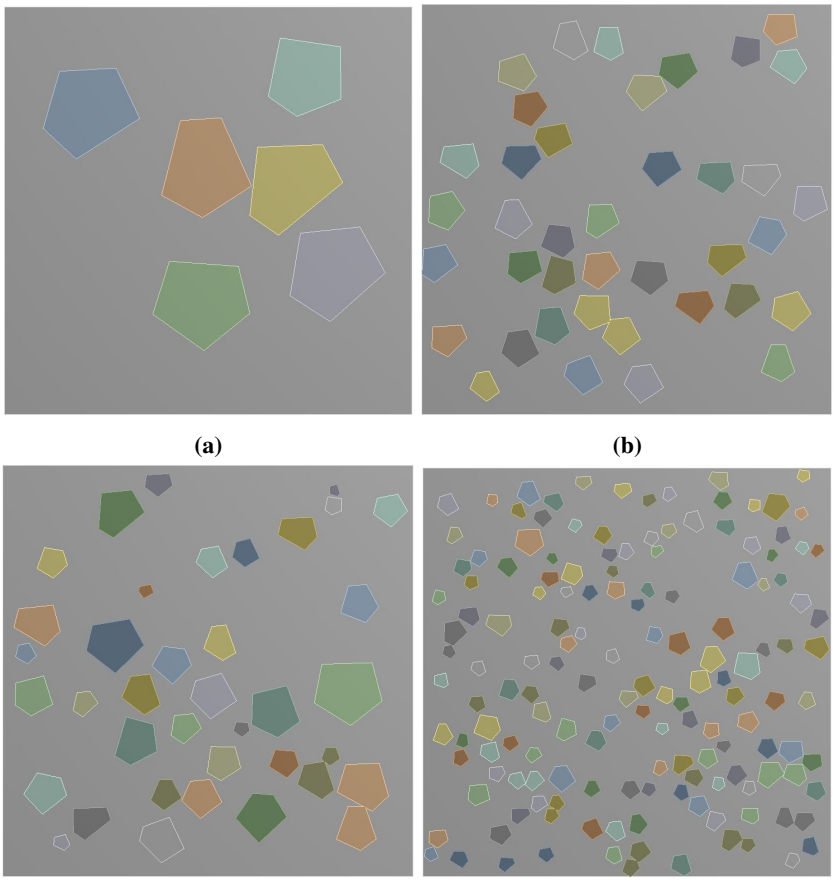

Fig. 6.15 Composites used in the model, parameters given in

dispersion of particulates are thought to lead to greater increases in stiffness. Interestingly the values found differs only marginally to the simulated pristine material, which in Section 5.2 was found to have a stiffness of around $1340\,\mathrm{MPa}$. This is actually consistent with what was seen in tensile tests, where the inclusion of graphene in PP prompted only a small increase in stiffness, albeit of higher magnitude than what is observed here. This suggests other effects, not accounted for in the model, are contributing to the changes in mechanical properties observed in tensile tests. When the size distribution of agglomerates is varied, some minor variances in stiffness are seen, and interestingly there have even been a reduction, seen for composite (a). In tensile tests, a reduced stiffness might suggest microcracks have been formed prematurely, allowing for the material to strain excessively, but this effect have not been included in these simulations. Where this excessive strain is coming from in the model presented, have not been possible to determine. The rest of the composites show increases in stiffness, where (b) and (c) have almost the same stiffness, possibly due to the similarity of the agglomeration characteristics. Composite (d) exhibits the highest increase in stiffness and the lowest degree of agglomeration, suggesting the benefits of having properly dispersed filler material in the composite. This may be explained by the way some sources of strain is allowed to "wander" through the material. When a force is a applied to the composite, strain is induced locally somewhere in the composite, evidently in the matrix, as it has the lowest stiffness. Nearby nodes are then affected by this strain, allowing for the strain to propagate throughout the composite. However, when several smaller particulates are distributed throughout the material, the strain propagation is more likely to be hindered, as compared to a material containing larger particulates, which are not as evenly distributed.

Chapter 7

Conclusion

The work in presented in this report revolved around investigating the effects of agglomeration on the mechanical properties of PP/GO composites. A functionalisation procedure where stearic acid was attached to the filler with the aid of a NaOH catalyst, was carried out to change the degree of agglomeration observed in composites. Further experiments studied the phenomena related to agglomeration in more detail, and a continuum mechanical model was developed to study the effect of agglomeration degree in the composites. From optical microscopy observations on the tensile specimens produced, there was no appreciable change in agglomeration degree, following the functionalisation of GO. This was also the case in previous work[1], and it seems the functionalisation procedure, whether catalysed or not, is not able to influence the agglomeration characteristics. Using PVA as a matrix material, and the accompanying "wet" mixing procedure, showed a much lesser degree of agglomeration, suggesting either good polymer-filler affinity or the specific mixing procedure is required for reducing agglomeration. However, since the functionalisation procedure would have influenced the polymer-filler affinity in the PP composites, it seems the mixing procedure is most influential. The degree to which the functionalisation had occurred in the procedure employed was only somewhat confirmed by infrared spectroscopy. Bands belonging to stearic acid were found in filler samples, but they were difficult to discern due to the generally high absorbance across the spectrum. Furthermore, it could not be determined definitively if all adsorbed stearic acid had been removed from the samples, however the tensile tests would suggest an appreciable degree of functionalisation had occurred. In tensile tests it was found that pristine GO could raise the stiffness of the composite to a minor degree, but did not change the ultimate tensile strength. Here it was also seen that functionalised GO could greatly increase the composite stiffness, of around 60%, hinting at the fact that agglomeration degree is not as influential as other factors, because both composites had the same degree of agglomeration. Results from the developed model suggested otherwise, as composites with better dispersion characteristics saw greater increases in stiffness, compared to composites with poor dispersion, although the magnitude of the increases were not near those observed in tensile tests. Tensile tests of PVA/GO composites showed a five-fold increase in stiffness, which hinted at the effects GO can have on a composite, provided it is properly dispersed and has good interphasial bonding. In one of the smaller experiments, regarding the effects sonication has on agglomeration, it was seen that the sonication time impacted the particle size distribution more. Suspensions subject to shorter sonication times had a lower concentration of small particles, whereas the sonication intensity seemed not to have any appreciable effect on the suspensions. The other small experiment, the timelapse of agglomeration in a PVA/GO solution, provided some key insights into the agglomeration behaviour. GO generally did not prefer to agglomerate in this solution, meaning the particle size distribution was governed mostly by the preceeding processing steps, i.e. exfoliation and sonication. As water evaporates from the solution, small particulates seem to become locked in place by the PVA, as opposed to disperse evenly on the substrate below. This means particulates are not able to move together and form agglomerates, and this could be crucial to ensuring a good degree of dispersion in a composite. Since PP composites are produced by allowing the GO particles to move close to each other and form agglomerates in the drying step, the agglomeration is poor and governed mainly by the melt mixing process. In the timelapse experiment, several larger particles were also observed, thought to be unexfoliated graphite particles, and these were also found in the sonication experiment.

So the exfoliation procedure can probably produce appreciably small GO particles as is, albeit some unwanted graphite particles are most likely still present. The main contributor of the poor agglomeration is the manner in which the GO is added to the PP, namely the drying step. The functionalisation procedure was not able to influence this step, although it could influence other properties of the composite, and perhaps poor agglomeration is not as detrimental as previously implied.

Bibliography

[1] Patrick Kruse. *Characterising the quality of graphene produced using three types of graphite in electrochemical exfoliation and its incorporation as a polypropylene nanofiller by functionalisation using stearic acid*, 2019.

[2] YJ Dappe, Miguel A Basanta, F Flores, and J Ortega. Weak chemical interaction and van der waals forces between graphene layers: A combined density functional and intermolecular perturbation theory approach. *Physical Review B*, 74(20):205434, 2006.

[3] William S. Hummers and Richard E. Offeman. Preparation of Graphitic Oxide. *Journal of the American Chemical Society*, 80(6):1339, mar 1958.

[4] Mikael Larsen. Mechanical properties of functionalised graphite oxide pp nanocomposites. *21st International Conference on Composite Materials*, aug 2017.

[5] Marc H. Hansen. Mechanical properties of functionalized electrochemical exfoliated graphene in polypropylene. Master's thesis, Aalborg University, 2018.

[6] D.C. Rapaport and D.C.R. Rapaport. *The Art of Molecular Dynamics Simulation*. Cambridge University Press, 2004.

[7] R.G. Parr and W. Yang. *Density-Functional Theory of Atoms and Molecules*. International Series of Monographs on Chemistry. Oxford University Press, USA, 1994.

[8] Michele Meo and Marco Rossi. Prediction of Young's modulus of single wall carbon nanotubes by molecular-mechanics based finite element modelling. *Composites Science and Technology*, 66(11-12):1597–1605, sep 2006.

[9] Jixuan Gong, Lonny Thompson, and Gang Li. On the local and non-local plate models of single layer graphene. *International Journal of Solids and Structures*, 166:57–67, jul 2019.

[10] Mengxi Chen, Lin Hu, Ashwin Ramasubramaniam, and Dimitrios Maroudas. Effects of pore morphology and pore edge termination on the mechanical behavior of graphene nanomeshes. *Journal of Applied Physics*, 126(16):164306, 2019.

[11] Zhonghua Ni, Hao Bu, Min Zou, Hong Yi, Kedong Bi, and Yunfei Chen. Anisotropic mechanical properties of graphene sheets from molecular dynamics. *Physica B: Condensed Matter*, 405(5):1301–1306, mar 2010.

[12] Aningi Mokhalingam, Reza Ghaffari, Roger A. Sauer, and Shakti S. Gupta. Comparing quantum, molecular and continuum models for graphene at large deformations. *Carbon*, 159:478–494, apr 2020.

[13] C. D. Reddy, S. Rajendran, and K. M. Liew. Equilibrium configuration and continuum elastic properties of finite sized graphene. *Nanotechnology*, 17(3):864–870, 2006.

[14] Changgu Lee, Xiaoding Wei, Jeffrey W. Kysar, and James Hone. Measurement of the elastic properties and intrinsic strength of monolayer graphene. *Science*, 321(5887):385–388, 2008.

[15] Ahad Shoghmand Nazarloo, Mohammad Taghi Ahmadian, and Keikhosrow Firoozbakhsh. On the mechanical characteristics of graphene nanosheets: a fully nonlinear modified Morse model. *Nanotechnology*, 31(11):115708, 2020.

[16] Diogo Galhofo, Nuno Silvestre, Bruno Faria, and Cátia Guarda. Monotonic and hysteretic in-plane behaviour of graphene through an atomistic FE model. *Composites Part B: Engineering*, 156:310–318, jan 2019.

[17] Na Liu, Fang Luo, Haoxi Wu, Yinghui Liu, Chao Zhang, and Ji Chen. One-step ionic-liquid-assisted electrochemical synthesis of ionic-liquid-functionalized graphene sheets directly from graphite. *Advanced Functional Materials*, 18(10):1518–1525, 2008.

[18] Junzhong Wang, Kiran Kumar Manga, Qiaoliang Bao, and Kian Ping Loh. High-Yield Synthesis of Few-Layer Graphene Flakes through Electrochemical Expansion of Graphite in Propylene Carbonate Electrolyte. *J. Am. Chem. Soc*, 133, 2011.

[19] Benoît D.L. Campéon, Mitsuo Akada, Muhammed S Ahmad, Yasushi Nishikawa, Kazuma Gotoh, and Yuta Nishina. Non-destructive, uniform, and scalable electrochemical functionalization and exfoliation of graphite. *Carbon*, 158:356–363, 2020.

[20] Antonio Gamboa, Gérard L. Vignoles, and Jean Marc Leyssale. On the prediction of graphene's elastic properties with reactive empirical bond order potentials. *Carbon*, 89:176–187, aug 2015.

[21] Xiao Liu, Thomas H Metcalf, Jeremy T Robinson, Brian H Houston, and Fabrizio Scarpa. Shear modulus of monolayer graphene prepared by chemical vapor deposition. *Nano Letters*, 12(2):1013–1017, 2012.

[22] Jin Wu Jiang, Tienchong Chang, Xingming Guo, and Harold S Park. Intrinsic Negative Poisson's Ratio for Single-Layer Graphene. *Nano Letters*, 16(8):5286–5290, 2016.

[23] Jie Hou, Binghui Deng, Hanxing Zhu, Yucheng Lan, Yunfeng Shi, Suvranu De, Li Liu, Pritam Chakraborty, Fei Gao, and Qing Peng. Magic auxeticity angle of graphene. *Carbon*, 149:350–354, aug 2019.

[24] Ying Wang, Jincheng Lei, and Zishun Liu. Molecular dynamics study on the anisotropic Poisson's ratio of the graphene. *Diamond and Related Materials*, 93:66–74, mar 2019.

[25] Beidou Guo, Liang Fang, Baohong Zhang, and Jian Ru Gong. Graphene Doping: A Review. *Insciences Journal*, 1(2):80–89, 2011.

[26] Yasuhiro Yamada, Kazumasa Murota, Ryo Fujita, Jungpil Kim, Ayuko Watanabe, Masashi Nakamura, Satoshi Sato, Kenji

Hata, Peter Ercius, Jim Ciston, Cheng Yu Song, Kwanpyo Kim, William Regan, Will Gannett, and Alex Zettl. Subnanometer vacancy defects introduced on graphene by oxygen gas. *Journal of the American Chemical Society*, 136(6):2232–2235, 2014.

[27] Maoyuan Li, Tianzhengxiong Deng, Bing Zheng, Yun Zhang, Yonggui Liao, and Huamin Zhou. Effect of defects on the mechanical and thermal properties of graphene. *Nanomaterials*, 9(3), mar 2019.

[28] Tongwei Han, Tao Jiang, Xueyi Wang, Panpan Li, Linru Qiao, and Xiaoyan Zhang. Tuning the mechanical properties of nanoporous graphene: A molecular dynamics study. *Materials Research Express*, 6(9), 2019.

[29] Jinchun Yao, Yuxuan Xia, Shuhong Dong, Peishi Yu, and Junhua Zhao. Finite element analysis and molecular dynamics simulations of nanoscale crack-hole interactions in chiral graphene nanoribbons. *Engineering Fracture Mechanics*, 218, sep 2019.

[30] A. J. Stone and D. J. Wales. Theoretical studies of icosahedral C60 and some related species. *Chemical Physics Letters*, 128(5-6):501–503, 1986.

[31] Yujie Wei, Jiangtao Wu, Hanqing Yin, Xinghua Shi, Ronggui Yang, and Mildred Dresselhaus. The nature of strength enhancement and weakening by pentagong-heptagon defects in graphene. *Nature Materials*, 11(9):759–763, 2012.

[32] Asanka Weerasinghe, Andre R. Muniz, Ashwin Ramasubramaniam, and Dimitrios Maroudas. Mechanical properties of hydrogenated electron-irradiated graphene. *Journal of Applied Physics*, 120(12):124301, sep 2016.

[33] Q. X. Pei, Y. W. Zhang, and V. B. Shenoy. A molecular dynamics study of the mechanical properties of hydrogen functionalized graphene. *Carbon*, 48(3):898–904, mar 2010.

[34] T.A. Osswald and G. Menges. *Materials Science of Polymers for Engineers*. Hanser Publishers, 2003.

[35] Shuai Zhang, Tianbao Ma, Ali Erdemir, and Qunyang Li. Tribology of two-dimensional materials: From mechanisms to modulating strategies, 2019.

[36] Jing Wang, Xiaochuan Guo, Yan He, Mingjun Jiang, and Kecheng Gu. Tribological characteristics of graphene as grease additive under different contact forms. *Tribology International*, 127:457–469, 2018.

[37] Yuan-zhong Hu. *Commensurability*, pages 397–401. Springer US, 2013.

[38] Linfeng Wang, Tianbao Ma, Yuanzhong Hu, and Hui Wang. Understanding the atomic-scale friction in graphene: The distinction in behaviors of interlayer interactions during sliding. *Journal of Applied Physics*, 120(20):205302, 2016.

[39] Liang Xu, Tian Bao Ma, Yuan Zhong Hu, and Hui Wang. Vanishing stick-slip friction in few-layer graphenes: The thickness effect. *Nanotechnology*, 22(28), 2011.

[40] Manoj Tripathi, Firas Awaja, Rafael A. Bizao, Stefano Signetti, Erica Iacob, Guido Paolicelli, Sergio Valeri, Alan Dalton, and Nicola Maria Pugno. Friction and Adhesion of Different Structural Defects of Graphene. *ACS Applied Materials and Interfaces*, 10(51):44614–44623, 2018.

[41] R. J. Dikken, B. J. Thijsse, and L. Nicola. Friction of atomically stepped surfaces. *Phys. Rev. B*, 95:104106, Mar 2017.

[42] Yong Chen, Shiwei Wang, Lu Xie, Pengzhe Zhu, Rui Li, and Qing Peng. Grain size and hydroxyl-coverage dependent tribology of polycrystalline graphene. *Nanotechnology*, 30(38), 2019.

[43] Jae Hyeon Ko, Sangku Kwon, Ik Su Byun, Jin Sik Choi, Bae Ho Park, Yong Hyun Kim, and Jeong Young Park. Nanotribological properties of fluorinated, hydrogenated, and oxidized graphenes. *Tribology Letters*, 50(2):137–144, 2013.

[44] S. Javan Nikkhah, M. R. Moghbeli, and S. M. Hashemianzadeh. Investigation of the interface between polyethylene and functionalized graphene: A computer simulation study. *Current Applied Physics*, 15(10):1188–1199, oct 2015.

[45] Yikuang Jin, Fangli Duan, and Xiaojing Mu. Functionalization enhancement on interfacial shear strength between graphene and polyethylene. *Applied Surface Science*, 387:1100–1109, nov 2016.

[46] Cheng Lv, Qingzhong Xue, Dan Xia, Ming Ma, Jie Xie, and Huijuan Chen. Effect of chemisorption on the interfacial bonding characteristics of graphene-polymer composites. *Journal of Physical Chemistry C*, 114(14):6588–6594, 2010.

[47] Tianjiao Li, Zhaoxu Meng, and Sinan Keten. Interfacial mechanics and viscoelastic properties of patchy graphene oxide reinforced nanocomposites. *Carbon*, 158:303–313, mar 2020.

[48] Akarsh Verma, Avinash Parashar, and M. Packirisamy. Effect of grain boundaries on the interfacial behaviour of graphene-polyethylene nanocomposite. *Applied Surface Science*, 470:1085–1092, mar 2019.

[49] YA Badr, KM Abd El-Kader, and Rasha M Khafagy. Raman spectroscopic study of cds, pva composite films. *Journal of applied polymer science*, 92(3):1984–1992, 2004.

[50] Sun-Young Lee, D Jagan Mohan, In-Aeh Kang, Geum-Hyun Doh, Soo Lee, and Seong Ok Han. Nanocellulose reinforced pva composite films: effects of acid treatment and filler loading. *Fibers and Polymers*, 10(1):77–82, 2009.

[51] Ruixia Hou, Guohua Zhang, Gaolai Du, Danxia Zhan, Yang Cong, Yajun Cheng, and Jun Fu. Magnetic nanohydroxyapatite/pva composite hydrogels for promoted osteoblast adhesion and proliferation. *Colloids and Surfaces B: Biointerfaces*, 103:318–325, 2013.

[52] Lu Zhang, Zhipeng Wang, Chen Xu, Yi Li, Jianping Gao, Wei Wang, and Yu Liu. High strength graphene oxide/polyvinyl

alcohol composite hydrogels. *Journal of Materials Chemistry*, 21(28):10399–10406, 2011.

[53] Shuhong Wang, Cheng Wang, Bin Zhang, Zhiyao Sun, Ziyang Li, Xiankai Jiang, and Xuduo Bai. Preparation of fe3o4/pva nanofibers via combining in-situ composite with electrospinning. *Materials Letters*, 64(1):9–11, 2010.

[54] M.P. Stevens. *Polymer Chemistry: An Introduction*. Oxford University Press, 2009.

[55] Maria Peresin et al. Novel lignocellulosic composites. -, 2011.

[56] Zheng Peng and Ling Xue Kong. A thermal degradation mechanism of polyvinyl alcohol/silica nanocomposites. *Polymer Degradation and Stability*, 92(6):1061–1071, 2007.

[57] Natalja Jelinska, Martins Kalnins, Velta Tupureina, and Anda Dzene. Poly (vinyl alcohol)/poly (vinyl acetate) blend films. *Scientific Journal of Riga Technical University*, 21(1):55–61, 2010.

[58] C Bartholome, P Miaudet, A Derré, M Maugey, O Roubeau, C Zakri, and P Poulin. Influence of surface functionalization on the thermal and electrical properties of nanotube–pva composites. *Composites Science and Technology*, 68(12):2568–2573, 2008.

[59] Ping'an Song, Zhiguang Xu, and Qipeng Guo. Bioinspired strategy to reinforce pva with improved toughness and thermal properties via hydrogen-bond self-assembly. *ACS Macro Letters*, 2(12):1100–1104, 2013.

[60] M Krumova, D Lopez, R Benavente, C Mijangos, and JM Perena. Effect of crosslinking on the mechanical and thermal properties of poly (vinyl alcohol). *Polymer*, 41(26):9265–9272, 2000.

[61] Jiajie Liang, Yi Huang, Long Zhang, Yan Wang, Yanfeng Ma, Tianyin Guo, and Yongsheng Chen. Molecular-level dispersion of graphene into poly (vinyl alcohol) and effective reinforcement of their nanocomposites. *Advanced Functional Materials*, 19(14):2297–2302, 2009.

[62] Thaís MC Maria, Rosemary A De Carvalho, Paulo JA Sobral, Ana Mônica BQ Habitante, and Javier Solorza-Feria. The effect of the degree of hydrolysis of the pva and the plasticizer concentration on the color, opacity, and thermal and mechanical properties of films based on pva and gelatin blends. *Journal of Food Engineering*, 87(2):191–199, 2008.

[63] W Chartarrayawadee, R Molloy, A Ratchawet, N Janmee, M Butsamran, and K Panpai. Fabrication of poly (lactic acid)/graphene oxide/stearic acid composites with improved tensile strength. *Polymer composites*, 38(10):2272–2282, 2017.

[64] Su Jin Han, Hyung-Il Lee, Han Mo Jeong, Byung Kyu Kim, Anjanapura V Raghu, and Kakarla Raghava Reddy. Graphene modified lipophilically by stearic acid and its composite with low density polyethylene. *Journal of Macromolecular Science, Part B*, 53(7):1193–1204, 2014.

[65] Facundo Ignacio Altuna, Cristina Elena Hoppe, and Roberto Juan José Williams. Epoxy vitrimers: the effect of transesterification reactions on the network structure. *Polymers*, 10(1):43, 2018.

[66] Werner J Blank, ZA He, and Marie Picci. Catalysis of the epoxy-carboxyl reaction. *Journal of Coatings Technology*, 74(926):33–41, 2002.

[67] Thomas Vidil, François Tournilhac, Simone Musso, Agathe Robisson, and Ludwik Leibler. Control of reactions and network structures of epoxy thermosets. *Progress in Polymer Science*, 62:126–179, 2016.

[68] Bethany A Wellen, Evan A Lach, and Heather C Allen. Surface pka of octanoic, nonanoic, and decanoic fatty acids at the air–water interface: applications to atmospheric aerosol chemistry. *Physical Chemistry Chemical Physics*, 19(39):26551–26558, 2017.

[69] A Jha, D Banerjee, and KK Chattopadhyay. Improved field emission from amorphous carbon nanotubes by surface functionalization with stearic acid. *Carbon*, 49(4):1272–1278, 2011.

[70] Sukhvir Kaur Bhangu and Muthupandian Ashokkumar. Theory of sonochemistry. In *Sonochemistry*, pages 1–28. Springer, 2017.

[71] Muthupandian Ashokkumar et al. *Theoretical and experimental sonochemistry involving inorganic systems*. Springer Science & Business Media, 2010.

[72] Zhiwei Huang, Zijie Li, Lirong Zheng, Limin Zhou, Zhifang Chai, Xiaolin Wang, and Weiqun Shi. Interaction mechanism of uranium (vi) with three-dimensional graphene oxide-chitosan composite: Insights from batch experiments, ir, xps, and exafs spectroscopy. *Chemical Engineering Journal*, 328:1066–1074, 2017.

[73] Hae-Kyung Jeong, Leyla Colakerol, Mei Hua Jin, Per-Anders Glans, Kevin E Smith, and Young Hee Lee. Unoccupied electronic states in graphite oxides. *Chemical Physics Letters*, 460(4-6):499–502, 2008.

[74] Hae-Kyung Jeong, Yun Pyo Lee, Mei Hua Jin, Eun Sung Kim, Jung Jun Bae, and Young Hee Lee. Thermal stability of graphite oxide. *Chemical Physics Letters*, 470(4-6):255–258, 2009.

[75] CH Manoratne, SRD Rosa, and IRM Kottegoda. Xrd-hta, uv visible, ftir and sem interpretation of reduced graphene oxide synthesized from high purity vein graphite. *Material Science Research India*, 14(1):19–30, 2017.

[76] M Mermoux, Y Chabre, and A Rousseau. Ftir and 13c nmr study of graphite oxide. *Carbon*, 29(3):469–474, 1991.

[77] Rabin Bissessur and Stephen F Scully. Intercalation of solid polymer electrolytes into graphite oxide. *Solid State Ionics*, 178(11-12):877–882, 2007.

[78] S Chaiyakun, N Witit-Anun, N Nuntawong, P Chindaudom, S Oaew, C Kedkeaw, P Limsuwan, et al. Preparation and characterization of graphene oxide nanosheets. *Procedia Engineering*, 32:759–764, 2012.

[79] D. Lin-Vien. *The Handbook of Infrared and Raman Characteristic Frequencies of Organic Molecules*. Academic Press, 1991.

Chapter A

Appendix

A.1 Preliminary experiments

In these experiments, wet mixing is attempted as an alternative to conventional melt mixing. Wet mixing involves the dissolution of both matrix and filler material in separate (or similar) solvents, mixing of the solutions followed by removal of the solvent. PP was previously used as matrix material, but can only be dissolved in volatile solvents at high temperatures, complicating the process. As an alternative, PVA is chosen for initial testing, because it easily dissolves in water, which GO can form a stable suspension in.

$1\,\mathrm{g}$ of PVA was dissolved in $20\,\mathrm{mL}$ deionized water and added to a suspension of $10\,\mathrm{mg}$ GO in $10\,\mathrm{mL}$ water (providing a polymer composite of $1\,\mathrm{wt}\%$ GO). The solution was stirred for $60\,\mathrm{min}$ and a few drops were dispersed under the bottom of a glass beaker and left to dry at room temperature. The next day, a film of PVA/GO with a thickness of around $25\,\mu\mathrm{m}$ could be peeled from the beaker and inspected in a microscope. A tensile specimen of PP/GO prepared by melt mixing was also cut to size and polished down to a thickness of $200\,\mu\mathrm{m}$ for comparison. Images of composite surfaces were acquired using transmissive light microscopy and can be seen in Fig. A.1

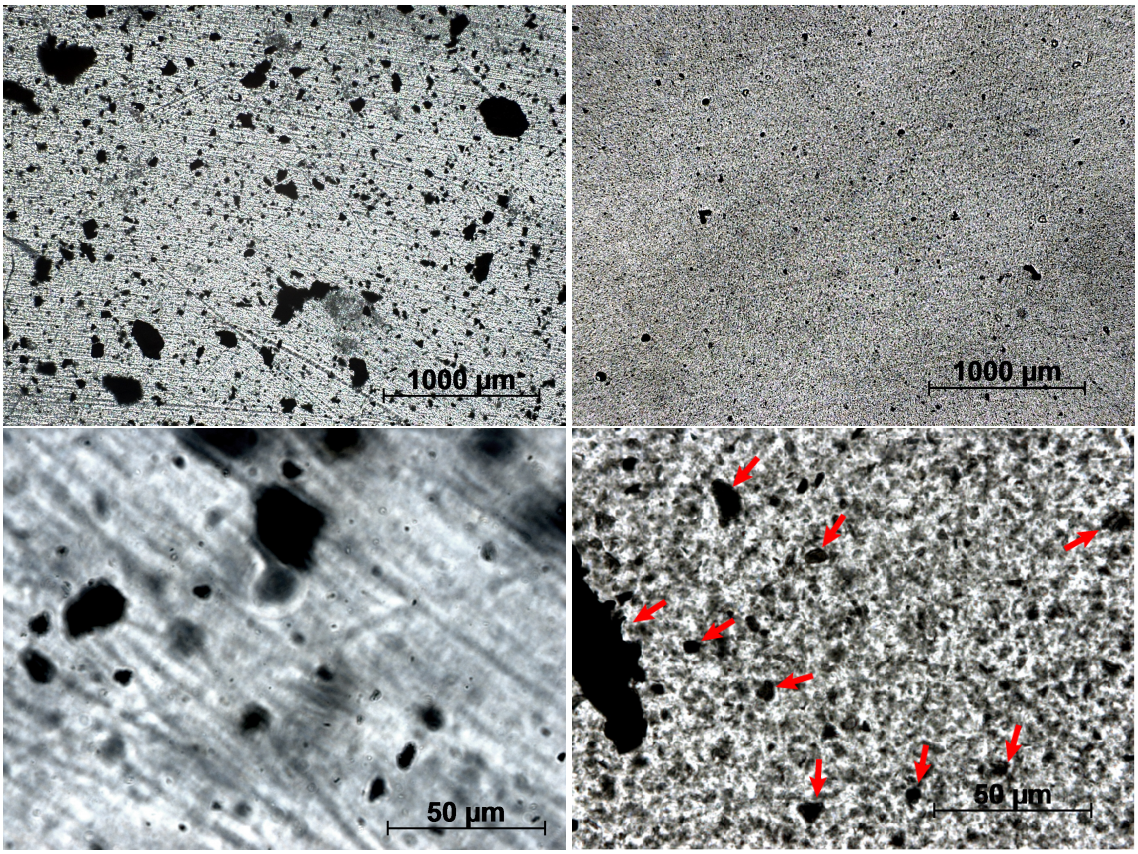

Fig. A.1 Transissive LOM images of the composites at both 5X and 100X magnification. Left: PP/GO, right: PVA/GO.

Looking at the PP composite at 5X magnification; several large GO agglomerates are clearly visible in black while the bulk plastic, between particles, appears white/transparent. Agglomerates are also clearly distinguishable at 100X magnification and it seems the specimen contains both small particles of around $5\,\mu\mathrm{m}$ and large particles up to $250\,\mu\mathrm{m}$ in diameter. Inspecting the PVA/GO composite, the particles are

generally much smaller even at 5X magnification and the bulk plastic has gotten a faint grey tint. Both PVA and PP have a transparent/white appearance in pristine condition. The discoloration could be the result of finely dispersed GO particles smaller than can be clearly distinguished using LOM. This is apparent at 100X magnification as the greyish tint makes it difficult to distinguish agglomerates from the background on the picture shown. However, these could be identified looking directly through the microscope eyepiece, and some have been marked with red arrows. In general, identifiable particles have a diameter in the range of 3-75 µm, while the background is thought to have smaller particles still.

So a clear improvement is seen in the filler dispersion following wet mixing, seen by the overall decrease in particle size and the grey tint acquired by the composite. This is thought to be related to the small particle size present in the GO/water suspension following its sonication, and these are not allowed to agglomerate while the water is evaporating. Particles are locked in place by PVA molecules as the PVA/GO suspension becomes a slurry and eventually a solid. Whether the higher particle size limit is governed by the particle size in the GO/water suspension or the agglomeration during water evaporation in the PVA/GO mixture is unknown. Perhaps agglomeration is prevented because oxide groups on GO can form hydrogen bonds with the hydroxyl groups on PVA. Further testing have to be carried out in order to determine how much either mechanism is contributing to final the degree of filler dispersion.

In any case, the wet mixing process seemed promising, so an attempt at repeating the process using PP is carried out. Selecting the solvent for the process is the tricky part, because it has to be able to dissolve PP while also providing a somewhat stable suspension with GO. The solvent might also impart irreversible damage on the macromolecules, rendering the plastic weaker, which of course is not desirable. Decalin is known, from experience, to dissolve PP at elevated temperatures, but GO does not easily disperse in the solvent. Tetrahydrofuran might also be able to dissolve PP, but GO disperses just as bad in this solvent, so decalin is chosen for these experiments and possible degradation effects caused by the solvent are ignored for now.

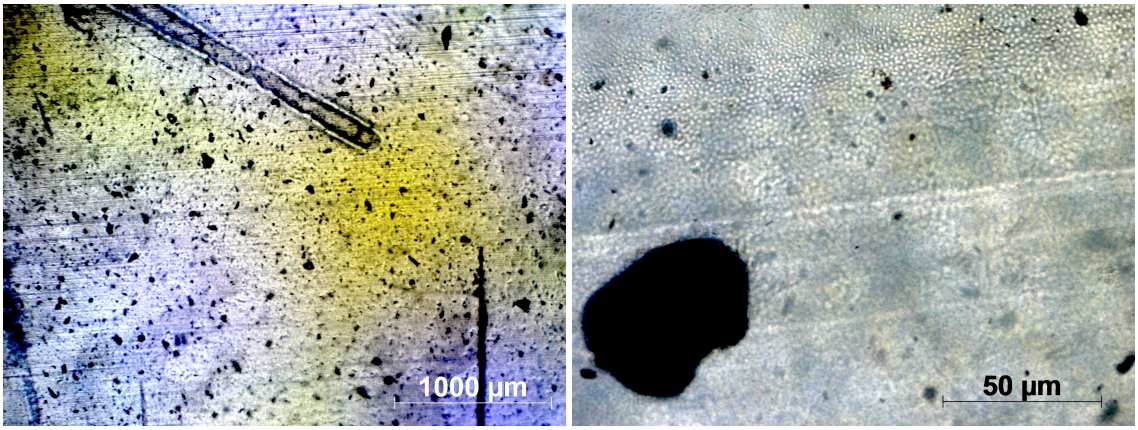

Fig. A.2 Transmission LOM images of the composites at both 5X and 100X magnification. Left: PP/GO, right: PVA/GO.

1 g of PP (Moplen HP400R) was dissolved in 25 mL decalin under heating. 10 mg GO was attempted suspended in 10 mL decalin, which after one hour of sonication had dispersed only a small amount of the GO, and a large piece of solid GO was still visible in the solution. Still, the suspension was added to the decalin/PP solution and stirred for a couple of minutes and this solution was then dispersed on the bottom of a glass beaker. The decalin had evaporated upon inspection the next day and only cracked plastic residue was left behind, which was scraped off and distributed on aluminium foil. The plastic was heated in an oven at around 180 °C for 60 min to both melt the plastic and ensure all the decalin was gone. The produced PP films had a thickness of ∼400 µm, gotten brittle and attained a slight yellow discoloration, probably from

chemical decomposition or from prolonged heating. In any case, the films were inspected in a microscope, seen on Fig. A.2. The general agglomerate size seem to have decreased, as compared to the dry-mixed PP composite, which could be considered an improvement, if the concentration of GO was comparable. Since the GO only dispersed partially in the decalin suspension, the concentration of filler is expected to be much lower than for the dry-mixed PP/GO composites, and less agglomerates can have formed as a result. Furthermore, compared to the PVA/GO composite, no grey tinting of the bulk plastic has occurred, meaning no appreciable dispersion has been achieved using this type of wet mixing.

A.2 Moplen HP400R datasheet

Technical Data Sheet

Moplen HP400R

Polypropylene, Homopolymer

Product Description

Moplen HP 400 R is a homopolymer polypropylene used by customers for injection moulding applications. It exhibits a high fluidity combined with a good stiffness.
Moplen HP 400 R is suitable for food contact.

Regulatory Status

For regulatory compliance information, see *Moplen* HP 400 R Product Stewardship Bulletin (PSB) and Safety Data Sheet (SDS) .

This grade is not intended for medical and pharmaceutical applications.

Status	Commercial: Active
Availability	Africa-Middle East; Europe
Application	Furniture; Housewares
Market	Consumer Products
Processing Method	Compounding; Injection Molding
Attribute	Medium Flow; Medium Stiffness

Typical Properties	Nominal Value	Units	Test Method
Physical			
Melt Flow Rate, (230 °C/2.16 kg)	25	g/10 min	ISO 1133-1
Density, (23 °C)	0.90	g/cm³	ISO 1183-1
Mechanical			
Tensile Modulus	1350	MPa	ISO 527-1, -2
Tensile Stress at Yield	32	MPa	ISO 527-1, -2
Tensile Strain at Break	>50	%	ISO 527-1, -2
Tensile Strain at Yield	10	%	ISO 527-1, -2
Impact			
Charpy Impact Strength - Notched, (23 °C, Type 1, Edgewise, Notch A)	3	kJ/m²	ISO 179
Hardness			
Ball Indentation Hardness, (H 358/30)	70	MPa	ISO 2039-1
Thermal			
Vicat Softening Temperature, (A50)	154	°C	ISO 306
Heat Deflection Temperature B, (0.45 MPa, Unannealed)	90	°C	ISO 75B-1, -2